Regional analysis of the 2015-16 Lower Mekong River basin drought using NASA satellite observations

Venkataraman Lakshmi[1], Manh-Hung Le[2, 3, *, +], Benjamin D. Goffin[1], Jessica Besnier[1], Hung T. Pham[4], Hong-Xuan Do[5, 6], Bin Fang[1], Ibrahim Mohammed[2, 3], John D. Bolten[2]

[1] *Department of Engineering Systems and Environment, University of Virginia, Charlottesville, VA 22904, USA.*

[2] *Hydrological Sciences Laboratory, NASA Goddard Space Flight Center, Greenbelt, MD 20771, USA.*

[3] *Science Applications International Corporation, Greenbelt, MD 20771, USA.*

[4] *The University of Danang - University of Science and Technology, Da Nang, Vietnam*

[5] *Faculty of Environment and Natural Resources, Nong Lam University - Ho Chi Minh City, Ho Chi Minh City, Vietnam*

[6] *Center for Technology Business Incubation, Nong Lam University - Ho Chi Minh City, Ho Chi Minh City, Vietnam*

**Corresponding author: manh-hung.le@nasa.gov*

+Former affiliation at Department of Engineering Systems and Environment, University of Virginia, Charlottesville, VA 22904, USA.

Submitted to Journal of Hydrology Regional Studies

February 2023

Abstract

Study Region

Lower Mekong River Basin (LMRB)

Study focus

Satellite remote sensing products are widely used for monitoring droughts. Using NASA satellite sensors of precipitation (Global Measurement Mission, GPM), soil moisture (Soil Moisture Active and Passive, SMAP), and terrestrial water storage (Gravity Recovery and Climate Experiment, GRACE), this study evaluates the historical drought in the LMRB during 2015-16. SMAP soil moisture was validated against *in-situ* soil moisture, and GPM precipitation and SMAP soil moisture were cross-validated with streamflow observations. The spatiotemporal dynamics of soil moisture were also examined in different ranges of catchment areas. In performing the analysis, we used lagged correlations between hydrological variables and the indices of the Standardized Precipitation Index (SPI) and Standardized Streamflow Index (SSI).

New hydrological insights for the regions

Spatio-temporal patterns of drought in 2015-16 were examined from the entire basin to small watersheds. A mismatch occurs when using GRACE data to study droughts in small watersheds (many of the small watersheds would be a fraction of the few 100 km^2 spatial resolutions of GRACE pixel). In smaller watersheds, hydrological drought (SSI) was closely defined with SMAP soil moisture downscaled to 1km rather than the meteorological drought index (SPI). By leveraging satellite-based observations across a range of spatial scales, this study highlights the utility of Earth observations in informing water resources and land management decisions at the regional scale.

Keywords: Mekong; GPM; SMAP; GRACE; downscaled SMAP; SPI; SSI

1. Introduction

Drought occurs naturally in any global climatic zone when the weather is warm and dry for an extended period of time (Tallaksen, 2000). Droughts can broadly be classified into four types: meteorological, hydrological, agricultural, and socioeconomic. The specific classification of droughts varies based on factors like the causes and consequences of drought, location, or field of study (West et al., 2019; WMO and GWP, 2016). For example, Thornthwaite (1947) divided droughts into four categories: permanent (when water demand exceeds supplied precipitation), seasonal (with rainy and dry seasons), contingent (irregular and variable rainfall), and invisible (can occur at any time). Conversely, Wilhite and Glantz (1985) classified drought into four groups: meteorological, hydrological, agricultural, and socioeconomic. Additionally, some studies have proposed different drought types, such as ecological drought (Bradford et al., 2020; Crausbay et al., 2018) and flash drought (Christian et al., 2019; Hu et al., 2021). Practically, all drought types are interrelated, and it is difficult to determine the start and end of each drought type (Ha et al., 2022; Son et al., 2021; West et al., 2019). For instance, a reduction in precipitation over time leads to meteorological drought. If this precipitation deficit continues, it can lead to reduced stream flow, lake levels, and groundwater, resulting in hydrological drought. The lack of rainfall and water supply causes soil moisture deficits, which are associated with agricultural droughts. Finally, socioeconomic drought occurs when water demand for social and economic activities exceeds water supply due to weather-related shortages, including impacts from meteorological, agricultural, or hydrological droughts (Elhag and Zhang, 2018). Among natural hazards, drought is one of the costliest ones because it reduces water availability which negatively affects agriculture and socioeconomic prosperity (Wilhite, 2000). Droughts are increasing in intensity and frequency as water resources are becoming limited across many regions in a warming climate, posing detrimental effects on society and our planet (Gudmundsson et al., 2021; Vörösmarty et al., 2010; Zhang et al., 2014; Zhongming et al., 2021).

Drought monitoring has traditionally relied on *in-situ* measurements but advances in earth observation technologies have transformed drought monitoring methods. Earth observations utilize different satellite missions to remotely sense different hydrological variables around the world. Precipitation is estimated by using some satellite missions/instruments, for instance Global Precipitation Measurement (GPM) (Huffman et al., 2020; Mohammed et al., 2018a; Mohammed et al., 2018b; Mohammed et al., 2018c), and Climate Hazards Group InfraRed Precipitation with Station data (CHIRPS) (Funk et al., 2015; Le et al., 2020b). The introduction of satellite-based precipitation products can enhance the spatio-temporal coverage of meteorological drought mapping and monitoring (Zhang et al., 2017). Moreover, agricultural drought monitoring research can utilize microwave sensors to acquire soil moisture content for characterizing soil moisture deficits (Bolten and Crow, 2012). Microwave sensors provide continuous coverage over large geographical areas and do not suffer from limitations associated with daylight availability and cloud coverage (Lakshmi, 2013). Surface soil moisture is extracted from various satellite missions equipped with active/passive microwave sensors such as Soil Moisture and Ocean Salinity (SMOS) (Kerr et al., 2001), or Soil Moisture Active Passive (SMAP) (Entekhabi et al., 2010). Additionally, remote sensing have enabled measurement of the Earth's total water storage in response to hydrological/groundwater droughts via the Gravity Recovery and Climate Experiment (GRACE) mission (Tapley et al., 2004). GRACE observed variations in terrestrial water storage (TWS) at all water storage locations (soil moisture, surface water, and groundwater). The GRACE satellite is unique as it measures below beneath the top five centimeters of the surface without being affected by surface conditions. Numerous studies have successfully used GRACE data to monitor hydrological droughts (Frappart et al., 2013; Rodell et al., 2009; Thomas et al., 2017). In Web of Science Search, drought-related publications based on satellite remote sensing have increased from fewer than 5 per year in 1982 to more than 300 per year in 2014 (West et al., 2019). Sheffield et al. (2018) discusses that remote sensing technologies have a significant role in improving water management throughout data-scarce regions. Overall, Earth observations have been increasingly used in recent decades

for drought monitoring, as their capacity to provide continuous observations over large spatial domains for several key hydrologic variables such as precipitation (Hou et al., 2014), soil moisture (Bolten et al., 2010; Bolten and Lakshmi, 2009; Chan et al., 2016), and terrestrial water storage (Syed et al., 2008) has been improving.

Over the Lower Mekong River Basin (LMRB), the agricultural system is sensitive to seasonal uncertainty and droughts are expected to increase in frequency and intensity. Around 70 percent of the population in the LMRB engages in agricultural activities (Abhishek et al., 2021). As the majority of agriculture in the region relies on rain, seasonality poses uncertainties about agricultural productivity and subsequent livelihood activities (Jones et al., 2003; MRC, 2003). The causes of droughts in the Mekong region are possibly (1) climate change, (2) low rainfall, (3) dry weather and high temperatures, (4) El Niño Southern Oscillation phenomenon, and (5) disagreements on water politics over Chinese dam construction and operation (Basist and Williams, 2020; Keovilignavong et al., 2021). In future drought projections, Thilakarathne and Sridhar (2017) demonstrated that drought severity and peak could be elevated significantly in the LMRB as analyzed from outputs from 15 global climate models (GCMs). Based on eight of the GCMs of CMIP6, Dong et al. (2022) reported that drought conditions will last longer during the dry season in most of the LMRB. Unfavorable climate conditions are projected in the Mekong Delta as increasing drought months (Mondal et al., 2022), or drought intensity (Li et al., 2021).

Remote sensing-based drought monitoring in the LMRB is an area of research that requires more attention. Meteorological and agricultural drought monitoring using satellite observations are among the most impactful topics (Son et al., 2012; Tran et al., 2019) (for more details, please see Table 1) but there is room for improvement. Most studies investigated remote sensing-based drought monitoring in large-scale regions. However, understanding of local hydrological information would be beneficial to inform local decision makers. Microwave remote sensing provides a promising way to understand drought condition

related to soil moisture deficits (Entekhabi et al., 2010). To date, there have been only a few studies assessing microwave remote sensing products over LMRB. This is due to the lack of *in-situ* soil moisture network to validate microwave remote sensing of soil moisture. There is only one previous study that has attempted to validate C-band microwave satellite-based soil moisture in the LMRB (Naeimi et al., 2013). However, this study used an indirect method through the evapotranspiration variable to validate soil moisture. Advanced soil moisture measurement using L-band microwave was attempted in the LMRB, but no *in-situ* validation has been previously discussed (Dandridge et al., 2020; Kang et al., 2021).

This research aims to demonstrate the relevance of NASA satellite observations for drought monitoring over the LMRB by (1) examination of historical drought conditions in 2015-16 using spaceborne data from precipitation, soil moisture, and terrestrial water storage; (2) assessment of high-resolution SMAP soil moisture to track the dynamics of the 2015-16 drought event at the watershed level; (3) cross-validation of soil moisture and precipitation- and streamflow-derived drought indices. We examined the 2015-16 drought, one of the worst natural disasters over the LMRB in recent years, causing tremendous impacts of socio-economic and livelihood in the region (MRC, 2019). We used GPM IMERG for precipitation, SMAP (9km) and its downscaled (1km) product for soil moisture, GRACE for terrestrial water storage. Also, to gain insights about drought conditions at regional scale, we focused on the entire basin, as well as the smaller watersheds. We obtained *in-situ* monthly streamflow over 16 catchments within LMRB and assessed co-variability of precipitation, soil moisture, and observed streamflow during the water year of 2015-16. There is no *in-situ* soil moisture network within LMRB but in the Southeast Asia region (similar biomass and climate), there are two available *in-situ* soil moisture networks. Therefore, we validated SMAP soil moisture products with these two networks. Finally, we cross-validated SMAP soil moisture products and GPM IMERG precipitation with a hydrological drought index derived from observed monthly streamflow.

[Insert Table 1]

2. Materials and Methods

2.1 Study areas

The Mekong River (795,000 km^2) is one of the largest rivers in Southeast Asia, originating from the Tibetan Plateau of China then flowing through six countries before ending to the East Sea of Vietnam. The Mekong is arguably one of the most important rivers in Southeast Asia as many regional economic sectors, including agriculture, energy, and fishery (Doan et al., 2020; Tran et al., 2021), heavily depend on water from this basin. In the Mekong River Basin, there are two main sub-basins: the Upper Mekong River Basin and the Lower Mekong River Basin. The Lower Mekong River Basin (LMRB) spans through Thailand, Lao PDR, Cambodia, and Vietnam and is made up of the Northern Highlands, the Khorat Plateau, the Tonle Sap basin, and the Mekong Delta, with a total landmass of about 600,000 km^2.

At the beginning of 2015, there was a severe drought across the LMRB that imposed negative impacts on the agricultural and fishing industries in the basin that led to significant economic losses (Binh et al., 2021; Guo et al., 2017; MRC, 2019; Park et al., 2022). In Thailand, the drought of 2015 caused the economic damage worth 1.7 billion USD. Additionally, more than 9.56 million people were affected in the 2015-16 drought, making this one of the costliest natural disasters in Southeast Asia over the past 20 years (Kang et al., 2021; MRC, 2019), even over the last 90 years in Mekong Delta (Kantoush et al., 2017).

2.2 In-situ datasets

2.2.1 Streamflow

In this study, streamflow records from tributaries of the Lower Mekong River basin were obtained from the Royal Irrigation Department (RID) and Vietnam Meteorological and Hydrological Administration

(VMHA). Both the RID and VMHA are officially responsible for monitoring river water level and discharge in Thailand and Vietnam, respectively. For RID data, we downloaded discharge records that are publicly accessible from the agency's website (http://water.rid.go.th/hyd; last accessed: February 3, 2022). For VMHA data, we obtained data directly from the authority (data is not publicly accessible). We identified basic metadata (i.e., geographical coordinates and catchment area) of each gauge using information available on the RID's website and from station documents provided by VMHA officers. To support our assessment of the 2015-16 drought event, we selected 16 catchments (the drainage area ranges from 248 to 10,878 km², with a median of 992 km²) based on the following criteria:

(a) Adequate data coverage: There are at least 20 values of monthly discharge for each calendar month. This ensures that we have sufficient data points to reliably estimate the distributions underlying our standardized streamflow index (SSI).
(b) There are no missing values during the period of 2015-16 so that we can have a complete drought condition for the event.
(c) There are no dams within the catchments. We use Stimson's Mekong Infrastructure Tracker (https://www.stimson.org/project/mekong-infrastructure/) as the basis to implement this assessment.

A geographical map of the LMRB and 16 catchments is shown in Figure 1, whereas a detailed description of the stream gauges is shown in Table 2.

[Insert Figure 1]

[Insert Table 2]

2.2.1 Soil moisture

There are no permanent sites or field campaigns to collect soil moisture in the LMRB. However, in Southeast Asia region with a similar climate and biomass as the LMRB, the International Soil Moisture Network has maintained two *in-situ* soil moisture networks within this region (Dorigo et al., 2021). These networks include MySMNet network (Malaysia) (Kang et al., 2019) and VDS network (Myanmar). The MySMNet has seven stations with data availability from May 2014 to December 2015 while VDS has four stations with data availability from June 2016 to February 2021. The major land use in the location of these two networks are savannas woody (MySMNet) and cropland (VDS). We used ground-based soil moisture measurements from these two networks to validate satellite-based SMAP soil moisture products during their overlap period. We obtained the *in-situ* soil moisture datasets from the International Soil Moisture Network (https://ismn.earth/en/).

2.3 Earth Observations datasets

2.3.1 GPM precipitation

The GPM (Global Precipitation Measurement) Core Observatory was launched on February 27, 2014. The satellite has Ka and Ku bands radar and a 13-channel microwave radiometer and is designed to provide new standard rainfall and snowfall observations globally every half-hour. The sensors include Dual-Frequency DPR (Precipitation Radar) and GMI (GPM Microwave Imager) and extend the measurement range of the TRMM (Tropical Rainfall Measuring Mission) (Hou et al., 2014; Huffman, 2016; Huffman et al., 2020). In this study, we obtained half-hour 0.1-degree GPM datasets from the latest version of IMERG (Integrated Multi-Satellite Retrievals for GPM) Final Run V6 (https://pmm.nasa.gov/data-access/downloads/gpm) ranging from 2001 to 2020. The GPM IMERG datasets are then accumulated on a monthly basis.

2.3.2 SMAP Soil Moisture

The Soil Moisture Active Passive (SMAP) is a soil moisture-focused mission that is operating in a near polar sun-synchronous orbit and with two overpasses - morning (6 a.m.) and afternoon (6 p.m.) and revisits every 2-3 days. The soil moisture estimates are retrieved from a 0-5 cm soil layer with a threshold of vegetation water content ≤ 5 kg/m^2, from an L-band radiometer at 1.41 GHz (Chan et al., 2016). The SMAP soil moisture retrievals can be downscaled by correlating the surface temperature difference to the soil moisture as a function of vegetation cover (Fang et al., 2013). For example, at the global scale, the 9km SMAP soil moisture is downscaled to 1km using GLDAS (Global Land Data Assimilation System) and MODIS (Moderate Resolution Imaging Spectroradiometer) land surface temperature and vegetation index. This downscaled soil moisture has been validated against field observations as well as aircraft data sets using 1,400 *in-situ* observing sites at a global scale (Fang et al., 2022). In this study, we obtained 9km SMAP Level 3 at the National Snow and Ice Data Center (NSIDC) (https://nsidc.org/data/smap) and downscaled SMAP 1km soil moisture from Fang et al. (2022).

2.3.3 GRACE Terrestrial Water Storage

We use GRACE RL06 product and GRACE-FO RL06 products for examination of the terrestrial water storage anomalies (TWSA) (Syed et al., 2008a). The data are global and are at a spatial resolution of 1 degree and a temporal repeat of one month for the terrestrial water anomalies. These anomalies depict the changes in the total water column of Earth which includes surface, sub-surface, and groundwater components (Syed et al., 2008a). GRACE has been used in global basins (Lakshmi et al., 2018) and Indian River Basins (Kansara and Lakshmi, 2021). In this study, the anomalies of terrestrial water storage are used (TWSA), obtaining from the Physical Oceanography Distributed Active Archive Center (PODAAC) (https://podaac.jpl.nasa.gov/datasetlist?search=GRACE%20(2002-2017)).

2.4 Methods

2.4.1. Areal value estimates from gridded Earth Observations datasets

Spatiotemporal changes of drought signal at a basin are usually monitored by assessing variabilities of precipitation, soil moisture, and terrestrial water storage derived from gridded satellite observations (Lakshmi et al., 2018; Voss et al., 2013; Wang et al., 2020). In this study, gridded monthly GPM IMERG precipitation, SMAP 9km soil moisture, downscaled SMAP 1km soil moisture, and GRACE TWSA products were extracted over the LMRB and sixteen watersheds during the water year from October 2015 to September 2016. Mean areal value for each variable was estimated to evaluate the ability of Earth observing satellites for monitoring drought across the study domain. We used Thiessen polygon areal weighted value (Le et al., 2022; Thiessen, 1911) to calculate mean areal value as considering the case that one pixel from Earth observations datasets may not be completely located within a target domain.

2.4.2 Lag-time analysis with cross-correlation

The cross correlation between precipitation and TWSA, and between soil moisture and TWSA were investigated to assess the relationship and lagged time between the variables during the drought event. The responsibility of TWSA to the changes in precipitation and/or reflection in soil moisture changes to the precipitation variability can exhibit the propagation time from the precipitation deficit to the soil water deficit followed by water deficits realized in deeper groundwater.

2.4.3 Monitoring drought dynamic with high-resolution SMAP soil moisture

The spatial resolution of Earth observation data has been a key issue in monitoring drought at catchment scale. For example, spatial resolution of SMAP soil moisture 9km is not ideal for detecting the changes in environmental variables and human activities (irrigation system) over sub-basins. The recent advancements in downscaling SMAP soil moisture (Fang et al., 2020; Fang et al., 2022), enable us to further explore soil moisture patterns. This study analyses the variability of the highest spatial-resolution satellite soil moisture

238 products (at global coverage) to offer a better understanding of changes in soil moisture under drought
239 conditions in several sub-basins with different catchment sizes.

240 *2.4.4 Drought indices from precipitation and streamflow*

241 We employed Standardized Precipitation Index (SPI) (McKee et al., 1993) and Standardized Streamflow
242 Index (SSI) (Farahmand and AghaKouchak, 2015; Telesca et al., 2012) to assess meteorological drought
243 and hydrological drought, respectively. The SPI relies primarily on the probability of precipitation whereas
244 the SSI is based on the probability of streamflow values. These indices were both chosen to investigate the
245 drought conditions and explore these two variables in relation to each other and the drought. SPI and SSI
246 are both normalized to zero mean and one standard deviation. These variables can be compared across time
247 and space with other SPI/SSI values as they are standardized. Since SPI and SSI are calculated separately
248 each month, the seasonal cycle should not affect them (Telesca et al., 2012). In each catchment, both indices
249 have been calculated at 1-month timescales with areal monthly GPM IMERG as input for SPI and monthly
250 observed streamflow as input for SSI. It must be noted that data length is essential to SPI and SSI
251 calculations. Therefore, we used 20 years of GPM IMERG data and +20 years of observed streamflow data
252 to calculate SPI and SSI, respectively. Then we extracted SPI and SSI values for the 2015-16 drought event.
253 We used Standardized Drought Analysis Toolbox (SDAT) (Farahmand and AghaKouchak, 2015) with two-
254 parameter gamma distribution and empirical distribution to estimate SPI and SSI time series, respectively.
255 A drought condition occurs when SPI/SSI is under -1 (McKee et al., 1993). Appendix 1 and Appendix 2
256 contain details regarding drought calculations and thresholds for SPI and SSI, respectively.

257 We assessed drought characteristics in terms of drought duration and drought severity. Drought durations
258 indicate total months in which drought indices values were under the drought threshold, whereas drought
259 severity is based on mean values of drought indices values during the drought duration periods (Le et al.,
260 2020a; Le et al., 2019). A drought episode occurred during the investigated period when at least two

consecutive months having values classified as drought condition. To this end, Table 3 summarizes the data used in this study and Figure 2 illustrates the overall methodology.

[Insert Table 3]

[Insert Figure 2]

3 Results and discussion

3.1 Assessment of SMAP soil moisture in the studied region

Over our region of interest, there is no prior work of validating SMAP soil moisture using *in-situ* measurements. Therefore, we conducted a validation study before applying SMAP soil moisture for our drought analysis. It is noted that we used two *in-situ* networks in the Southeast Asia region (similar climate and biomass as the LMRB) for the purpose of this evaluation. The pixel-to-point approach was used to match satellite-based soil moisture products with soil moisture measured from the *in-situ* networks.

We first evaluated absolute values of SMAP soil moisture against *in-situ* soil moisture measurements. To carry out this task, we normalized satellite-based soil moisture products, SMAP 9km (SM9) and its downscaled SMAP 1km (SM1), against the reference dataset (*in-situ* measurement) using the normalized equation (Draper et al., 2009; Kim et al., 2015) (please see Appendix 3 to see this equation in details). We observed a good correlation between both SMAP products and ground measurements as the pairwise points were around the 1-1 line of the scatter plots (Figure 3). The SM1 product exhibited a slightly higher correlation for both networks (Spearman correlation coefficient values are 0.903 and 0.865 for MySMNet and VDS, respectively).

[Insert Figure 3]

We further assessed delta changes between satellite-based soil moisture and *in-situ* soil moisture. In this evaluation, we did not apply the normalized equation. We used delta changes to cross-validate SMAP soil moisture in monitoring drought with standardized streamflow index (SSI) (see Section 3.5). We specifically focus on available data during the period of 2015-16 which overlaps with the investigated historical drought year. With this constraint, only MySMNet network has been used. The delta changes rates between *in-situ* soil moisture and SM9 soil moisture were found to be significantly related (CC = 0.48), and delta change rates between *in-situ* soil moisture and SM1 soil moisture were found to be significantly related (CC = 0.57) (for more details, please see Appendix 4).

There is concern about the use of SMAP soil moisture in forest cover regions. Most microwave satellite-based SM data over densely vegetated areas are masked out because biomass saturates the microwave signal, resulting in high errors and uncertainties for SM retrievals. In two field temperate forest canopy experiments in the northeast United States, Colliander et al. (2020) reported a Root Mean Square Difference (RMSD) of 0.047-0.057 m^3/m^3 and a Pearson correlation range of 0.75-0.85 for a parameterized emission model using the SMAP morning overpass. This study demonstrates the sensitivity of soil moisture under dense forest canopies, which had been uncertain due to a lack of representative reference data. In a global scale error assessment of soil moisture estimates, Kim et al. (2020) showed that model-based SM could provide accurate SM estimates than microwave satellite-based SM retrieval. In a study within the LMRB, microwave-based satellite estimates over cropland has more reasonable estimates than forest land (Naeimi et al., 2013).

In our study, half of the studied watersheds are dominated by cropland and shrubland land cover (Table 2). SMAP soil moisture estimates for these land cover types are generally reliable (Chan et al., 2016; Colliander et al., 2017). In Cambodia, where is dominated by cropland, Abhishek et al. (2021) used SMAP soil moisture as a reference for soil moisture outputs from their hydrological model. On the other hand, the

304 remaining watersheds have no dominant land cover (mainly mixed forest and grassland) (Table 2). In these
305 non-dominant land cover watersheds, dense vegetation coverage can be expected, and SMAP soil moisture
306 estimates may be uncertain. To minimize this risk of uncertainties, we chose not to use absolute SMAP soil
307 moisture values but delta changes when cross-validating SMAP soil moisture with other drought indices.

308 **3.2 Variability of precipitation, soil moisture and total water in the Lower Mekong River Basin**
309 **during 2015-16**

310 The Lower Mekong River Basin has faced a severe drought in 2015-16. Figure 4a shows the variability of
311 precipitation, soil moisture, and total water storage anomalies (TWSA) from October 2015 to September
312 2016. The patterns of precipitation, soil moisture and TWSA show a very interesting pattern of correlation
313 though lagged in time. The rainfall begins to decrease in the extreme northern and northeastern portions of
314 the basin in October 2015. This is followed by an almost complete drying of the basin albeit the southeastern
315 edge and the Vietnam Mekong Delta in November. By December 2015, the entire basin has less than 100
316 mm of precipitation and this continues into January through March 2016. In this period there are portions
317 of the basin that receive less than 10mm of precipitation in a month. However, this changes in April 2016
318 when the north-central portion of the basin receives precipitation more than 100 mm for the month and this
319 continues into May 2016 when the same region receives around 150 mm of precipitation. By June 2016,
320 the entire basin has over 150 mm of precipitation except for small regions in the north (June 2016) and in
321 the south and east (July 2016), south and west (August 2016) and extreme north (September 2016). It is
322 interesting to observe that soil moisture responds almost immediately to the changes in precipitation, but
323 the spatial patterns are not the same. The soil moisture is generally always greater than 0.4 in the Vietnam
324 Mekong Delta (the southern-most portion of the basin) and this is true even during periods of low
325 precipitation. The reason for this could be due to irrigation and/or standing water (the Vietnam Mekong
326 Delta is the heart of rice cultivation in the basin). If we compare the precipitation and soil moisture to the

spatial patterns of the terrestrial water storage anomalies, we see a lag of up to 2-3 months for recovery of the groundwater. This is expected as the increase in precipitation reflects almost immediately in the soil moisture but there is a time lag for this water to reach the aquifers and register in the TWSA.

In Figure 4b we see the basin averaged GPM precipitation (black line with circles), 9km SMAP soil moisture (red dashed line with squares) and the GRACE terrestrial water storage are plotted for October 2015 to September 2016. It is very clearly seen that the drop in the precipitation results in a corresponding drop of the soil moisture between October 2015 (150mm) and February 2016 (nearly zero). The precipitation starts to increase from around March 2016 (less than 10mm) to June 2016 (280mm) and the soil moisture follows (0.37 in October 2015 to 0.2 in March 2016). The precipitation shows a slight dip between June and July 2016 (280mm to 260mm), but the soil moisture continues its increase till July 2016 (0.38) following which the soil moisture shows a slight drop to August 2016 and then increases to September 2016. The precipitation on the other hand keeps on increasing between July and September 2016. The total water storage anomalies (TWSA) show a distinct lag with the precipitation and soil moisture. Whereas precipitation and soil moisture show almost monthly similarities, the TWSA decreases till May 2016 (-22mm) and only begins to recover in July and August 2016 (-5mm and +6mm respectively), thereby lagging the increase in precipitation by about 4 months (March – July). The correlation coefficients between precipitation and soil moisture are 0.91, between P and TWSA is 0.15 (no lag), 0.6 (lag 1 month) 0.7 (lag 2 months) and SM and TWSA is 0.5 (no lag), 0.8 (lag 1 month) and 0.7 (lag 2 months).

[Insert Figure 4]

Several prior studies confirm similar findings as ours from satellite sensors using diverse approaches. According to Abhishek et al. (2021), persistent dry spells were observed over Cambodia from 2015 to mid-2016 based on a modeling framework. Based on +30 years of reanalysis of precipitation data, Guo et al. (2017) found that 2015-16 were the driest in the LMRB, with drought-affected areas of up to 75% and serve

drought events lasted from April 2015 to July 2016. In a near-real-time drought monitoring experiment, Zhang et al. (2020) detected significant drought episodes during the 2015-16 dry season (November to April).

3.3 Examination of high spatial soil moisture variability for sub-catchments

One of the objectives of this work was to use satellite-based sensors to help understand the spatial and temporal propagation of the drought signal in small watersheds. Normally, studies of droughts have been limited to larger watersheds due to the low spatial resolution of the satellite observations. However, with the downscaling of the SMAP 9km soil moisture to 1km and its global availability, we are able to study smaller watersheds on the order of a few hundred square kilometers. In this sub-section we will examine the spatial and temporal propagation of the drought for five watersheds (Table 2) in the Lower Mekong River Basin with a range of areas on various river systems, viz., G.9 (river system: Name Mae Kok, area 386 km^2), Banyen (river system: Nam Mua area 638 km^2), Kh.28A (river system Khong, area 1,271 km^2), G.8 (river system: Name Mae Kok area 2,909 km^2) and I.14 (river system: Khong area 6,266 km^2). The choice of these watersheds also spans a range of geographical diversity and the availability of soil moisture datasets (Figure 1 and Table 2).

In Figure 5, soil moisture for catchment G.9 generally declines between October 2015 and April 2016 due to the decreasing precipitation noted in Figure 4b. Focusing on soil moisture at a spatial resolution of 1 km during this dry-out phase, we see a sub-pixel variability (in the SMAP 9 km soil moisture pixel) as a reflection of differential drying. This is especially true for February 2016 where some pixels show particular wetness (most likely due to irrigation). When comparing boxplots of soil moisture at different spatial resolutions, we observe a greater range in 1-km soil moisture from December 2015 through April 2016. A slight, subsequent decrease in soil moisture can be noted across both datasets in September 2016 (due to increased evaporation).

[Insert Figure 5]

Similar spatial and temporal patterns in the other four watersheds are examined in this section. In the case of the Banyen watershed (Figure 6), the soil moisture experiences a decline from January (0.37) to March (0.32). However, the variability of soil moisture at the spatial resolution of 1km shows more detailed information, especially in February 2016 with some locations still wet and others much drier. We also observe interesting nuance in soil moisture, especially in the southern part during the dry spell in April 2016 and localized wetness in September 2016.

[Insert Figure 6]

In the case of Kh.28A (Figure 7), the decrease in precipitation from October 2015 (100 m) to March 2016 (less than 10mm) is matched by the steady decline in soil moisture, especially at 1-km spatial resolution. The wetting up is not as obvious in the spatial soil moisture plots at Kh.28A as it was in previous catchments. However, we see that the soil moisture at 1 km consistently captures a greater range of variability in the boxplots. This is especially apparent in the month of July 2016 where the 1 km soil moisture shows a considerably higher range than that of 9 km soil moisture. This is possibly because the 1-km spatial resolution can pick up smaller, wetter irrigated patches.

[Insert Figure 7]

The G.8 (Figure 8) and I.14 (Figure 9) catchments exhibit similar patterns. The soil moisture at both the 9- and 1-km spatial resolution does not show a consistent watershed-wide decrease. In fact, some areas specifically in the northeast corner of the watershed show wetter areas between October 2015 to February 2016 (around 0.35), most likely caused by irrigation. Once again at these two catchments, we see that the soil moisture at 1 km provides a much wider range of information. This is true across the whole time series, during both the dry and wet periods.

[Insert Figure 8]

[Insert Figure 9]

Some hollow spots are visible on the spatial pattern maps of SMAP 1 km soil moisture (e.g., Figures 7 to 9). The MODIS land surface temperature (LST) data are contaminated by clouds, resulting in incomplete spatial coverage (Pham et al., 2021; Pham et al., 2018). Since LST is an independent variable in the 1km downscaling algorithm, its limited coverage impacts the SMAP 1km coverage.

3.4 Co-variability of precipitation, soil moisture and streamflow

Figure 10 provides the time series of the watershed spatially averaged monthly precipitation, runoff, soil moisture at 9- and 1-km spatial resolution for the five watersheds that we discussed in the previous section 3.2, viz., G.9, Banyen, Kh.28A, G.8 and I.14 in a, b, c, d and e respectively. The common thread among all these plots and watersheds is the fact that the watershed precipitation decreases similarly to the decreases in the larger Lower Mekong River Basin between October 2015 and March 2016 (between around 100mm in October 2015 to almost negligible in March 2016). Then the precipitation increases peaking at different times to different amounts in the different watersheds. In G.9 it is about 300mm for June 2016, 400m in Banyen in August 2016, 240mm in Kh.28A in June 2016, 250mm in June 2016 and 320mm in I.14. In some of these watersheds, the precipitation stays nearly constant after peaking or dropping.

The largest drop is in Banyen (Figure 10b) where the precipitation drops from 400m in August 2016 to 150mm in September 2016. The changes in the precipitation are reflected in the runoff – in all the watersheds, the runoff remains at very low amounts (less than 10mm) till May or June 2016 and then shows an increasing trend for the remainder of the year. In G.9 this increase is to about 50mm in September 2016; in Banyen, the increase is to 200mm for August 2016 and then a drop to 120mm for September 2016; for Kh.28A, there is a continual increase to 120mm in September 2016; there is a slight increase to about 40mm in G.8 in September 2016 and to 100m for I.14 in September 2016.

418 The soil moisture exhibits a temporal trend that tracks the precipitation very closely with an initial dry down
419 in all the watersheds between October 2015 to April 2016 followed by an increase to July 2016 followed
420 by a slight decrease (mirroring the precipitation). The minimum soil moisture in most of these watersheds
421 is reached in March or April 2016 and is close to 0.15. In almost all the watersheds, there is a deviation
422 from the negative trend between October 2015 to March/April 2016 with a local maximum in January 2016
423 most likely due to local irrigation in the watersheds. This upward bump is not seen in the spatial average
424 over the Lower Mekong River Basin (Figure 4b) where the soil moisture stays constant between December
425 2015 and January 2016. This increase varies in different watersheds with the largest increase observed in
426 the Banyen watershed (0.29 to 0.4) and a very slight increase in Kh.28A (0.18 and 0.21). There is a very
427 good agreement between the soil moisture at the 9- and 1-km spatial resolutions.

428 [Insert Figure 10]

429 Table 4 lists the watersheds, percentage of monthly available soil moisture for the 9- and 1-km spatial
430 resolution and the correlation between the variables, precipitation, runoff, soil moisture at 9- and 1-km
431 spatial resolutions (and all the cross correlations). This table demonstrates the high correlation between
432 precipitation, runoff, and soil moisture in almost all the watersheds except for Banyen, where the
433 correlations are generally low. One of the reasons for this could be the fact that there is irrigation and a use
434 of surface water for agricultural activities in this watershed and that disrupts the natural connections
435 between precipitation, runoff and soil moisture. With that exception, it is generally seen that most
436 correlations are greater than 0.7 and many of the correlations such as between precipitation and soil
437 moisture are in the 0.9 range. This demonstrates the effective use of satellite data in monitoring the drought
438 and linking it to observed stream flow. The high correlation between soil moisture at 9- and 1-km spatial
439 resolutions demonstrates the consistency of the two data sets.

440 [Insert Table 4]

3.5 Hydrological variability and relation with indices

Figure 11 presents variations of monthly precipitation anomalies and runoff anomalies along with relationship between SPI-1 and SSI-1 at 16 small watersheds during the water year of 2015-16. Generally, the runoff anomaly did not follow the same pattern as the anomaly in precipitation. The monthly averaged precipitation anomalies were greater than the long-run precipitation averages between December 2015 to January 2016 (20 mm) and between June to July 2016 (60 mm) (Figure 11a). On the other hand, the averaged runoff anomalies were lower than long-run runoff values for all months, especially from October-December 2015 (-30 mm) and August-September 2016 (-20mm) (Figure 11b). Drought duration and drought severity based on SPI and SSI reveal significant difference in drought characteristics obtained by these two drought indices (Table 5). SPI-based drought durations across catchments often lasted 2-3 months (average of 2.1 months), while SSI-based drought durations were longer, ranging from 2-12 months with an average of 5.4 months. In some catchments (G.9, Krongbuk, Kh.61, Kh.72, and G.8), there were more than two hydrological drought events during the period of 2015-16. In contrast, no hydrological drought events were observed in the Banyen and Kh.58A catchments during this period. The reason for this could be due to large water storage in aquifers that can discharge to streamflow in these catchments during drought development phase.

[Insert Table 5]

We also examined the cross correlation between SPI-1 and SSI-1 across small watersheds, observing the highest correlation coefficient (CC) varying from the lag of zero (lag 0) to the lag of two months (lag 2). Stream gauges that have the highest correlation between SPI and SSI with the lag 0, lag 1 and lag 2 are provided in Figure 11 c, d and e respectively. The highest correlation coefficient values are provided in the Supplementary S1. Among six stream gauges with lag of zero, there was only one gauge having statistically significant correlation located at the northeast of the LMRB (Figure 11c). Three of four stream gauges

464 located in the northwest, the west, and the southeast of the region have statistical significance of correlation
465 with propagation time of one month (Figure 11d). Whereas only two gauges in six stream gauges with
466 lagged time of two months distributed in the west of the basin (Figure 11e). The background map of Figure
467 11c-e shows the averaged TWSA during the water year 2015-16. The region with negative TWSA is drier
468 than normal conditions while positive TWSA region is wetter than normal conditions. The results are quite
469 surprising because it is contrary to what is known about links between catchment water storage capacity
470 and response time of catchment and hence lag time between SPI-1 and SSI-1. Major water stores (positive
471 TWSA) in catchment create long memory in hydrological system which makes long response time of
472 catchment and long propagation time between meteorological drought and hydrological drought as well.
473 However, longer lag times between SPI and SSI were found at dry catchments (Figure 11e) and fast
474 responding catchments had positive TWSA (Figure 11c). In other words, our understanding on large scale
475 observation from GRACE may not be true when we move to small size watersheds. In summary, the
476 differences in anomalies patterns between precipitation and runoff as well as differences in drought
477 characteristics between meteorological drought (SPI) and hydrological drought (SSI) suggest us that the
478 impact of precipitation on the severity of drought during 2015-16 was mild. Also, the coarse resolution of
479 GRACE data seems not truly to reflect the co-variability between precipitation and runoff at the small
480 watersheds.

481 [Insert Figure 11]

482 We introduced delta changes in months to cross-validate drought monitoring between SSI, SPI, and soil
483 moisture at 9km (SM9) and 1km (SM1). Delta change values have two benefits. First, catchments have flux
484 memories (precipitation, soil moisture, and streamflow). Flux changes between months could indicate
485 dryness or wetness signals. Second, we could use short-record soil moisture data in detecting
486 dryness/wetness signals since satellite-based soil moisture is only available for a short period (as compared

to the data length required for SPI and SSI). We only need current values to calculate delta changes, but not for long-term values. Figure 12 characterizes monthly changes in SSI, SPI, and soil moisture at 9km (SM9) and 1km (SM1). We only examined the co-variability of changes in SSI, SPI, SM9, and SM1 at five basins which almost have fully coverage of soil moisture (both 9km and 1km) at a monthly time step during the 2015-16 period (Figure 12a-e). Figure 12f presents cross correlation between monthly changes in SSI and monthly changes in SPI, SM9, and SM1. We found out that small catchments (G.9, Bye, and Kh.28A), the relationship between monthly changes in SSI could related to the changes in SPI, and soil moisture datasets, with a statistically significant at level 0.1. It is quite possible true as in the small watersheds, routing time is short and transfer the loss in precipitation and soil moisture to runoff can occur immediately. Among the relationships, the highest values were observed between monthly changes in SM1 and SSI, followed by SM9 and SSI, and SPI and SSI. It can be likely that soil moisture is a land surface parameter, which directly relates to runoff rather than precipitation (atmospheric parameter). The better of SM1 in liking with the changes in runoff also indicates its usefulness in accurately capturing dryness/wetness pixels in the small watersheds. On the other hand, at the large basins (G.8 and I.14), the relationship between monthly changes in SPI, SM9, and SM1 with monthly changes in SSI were weak. It may be due to the heterogeneity of land cover and complexity of routing process in the large catchments, causing non-linear process between the loss of precipitation and soil moisture to runoff.

[Insert Figure 12]

4 Conclusions

This study aims to assess whether NASA satellite sensors can be useful for monitoring a major drought event with spatially heterogeneous impacts. This work builds up on and complements traditional studies of droughts in two ways (1) most studies focus on use of drought metrics computed using precipitation (Standard Precipitation Index) or evapotranspiration (Standard Precipitation Evapotranspiration Index), but

this study uses explicitly precipitation, soil moisture and streamflow to track the evolution of the drought (2) most previous studies have focused on large watersheds while smaller watersheds have generally not been studied on an individual basic. We investigated various sensors with different spatial resolutions, including GRACE (100 kilometers), GPM (10 kilometers), SMAP (10 kilometers), and downscaled SMAP soil moisture (1 kilometer). The motivation of this study is to showcase the potential of using remotely sensed data to support water assessment over basins that are not monitored intensively or limited in data-sharing.

Our findings show that at the large scale (LMRB) precipitation, soil moisture, and total water are well correlated. Specifically, soil moisture and precipitation track each other and total water lags by a few months. At the catchment level, we observe a strong correlation between precipitation, soil moisture and streamflow. GRACE observations, however, do not reasonably reflect hydrological processes at the smaller catchment scales due to their low spatial resolution. For example, several dry catchments (negative TWS observed from GRACE) show longer lag time response between SSI and SPI, as compared to the wet catchments (positive TWS). From a theoretical perspective, less water stored in the catchment results in a short memory in the hydrological system. This enables a quick response time of the catchment and quick propagation between meteorological and hydrological droughts.

The availability of 1 km soil moisture observations highlights the ability to make water resources and land management decisions at the local scale. This high spatial resolution information can assist in specific agricultural decisions such as water availability during time of planting and/or harvest. Moreover, the benefits gained from devising operational drought monitoring framework with high spatial resolution soil moisture data are seen in strategic preparedness plans to combat droughts and mitigate their effects on the activities in the various sectors of the economy starting from the small scale up to large ones. Moreover, we find that monthly changes in the streamflow standardized index (SSI) are closely related to downscaled

1 km soil moisture at small catchment scales, as compared to the Standardized Precipitation Index (SPI). This opens a possibility of using 1 km soil moisture as a substitution of the hydrological drought SSI as its publicly available and easier to access than the ground runoff data.

The approach from this study can be further applied in other regions where episodes of drought are occurring at various spatial and temporal resolutions. The work presented here can be further refined to include upcoming high resolution surface water satellite products. Small scale detailed assessments of drought detection are expected to witness a breakthrough through the NASA Indian Space Research Organization (ISRO) Synthetic Aperture Radar (SAR) mission (NISAR products are available in 2023). NISAR is the first satellite mission that images the Earth in both L- and S-band radar frequencies and will produce surface water extent products over inland and coastal wetlands at least twice every 12 days with spatial resolution of 5-10 meters

Acknowledgements

This work was supported by the National Aeronautics and Space Administration (NASA) and the U.S. Department of State's Bureau of Oceans and International Environmental and Scientific Affairs, Office of Conservation and Water (IAA # 19318820Y0014). Jessica Besnier and Benjamin D. Goffin acknowledge that this work was also made possible through graduate fellowships from the National Science Foundation Research Traineeship Program and the Jefferson Scholars Foundation, respectively. Hong X. Do is supported by Nong Lam University - Ho Chi Minh City (grant for basic research No. CSCB21-MTTN-07) and the National Foundation for Science and Technology (NAFOSTED; grant for basic research in natural sciences and engineering No. 105.06-2021.17). Any opinions, findings, and conclusions or recommendations expressed in this work are those of the author(s) and do not necessarily reflect the views of the National Science Foundation Research Traineeship Program, Jefferson Scholars Foundation, NAFOSTED, National Aeronautics and Space Agency, and the U.S. Department of State's Bureau of Oceans and International Environmental and Scientific Affairs, Office of Conservation and Water.

Appendix

Appendix 1. Standardized Precipitation Index (SPI) calculation

This study calculated SPI at 1-month timescales (McKee et al., 1993). The three steps to calculate SPI are described as follows.

Step 1: Fitting distribution function for precipitation time series

$$X_{i,m}^{k} = \sum_{t=13-k+m}^{12} P_{i-1,t} + \sum_{t=1}^{m} P_{i,t} \tag{A1}$$

Where: k is time scale; i is year; m is month of year, P is precipitation.

The two-parameter Gamma distribution is used to fit the time series as follows.

$$G(x) = \int_{0}^{x} x^{\alpha-1} e^{-x/\beta} dx \tag{A2}$$

Where: α is shape parameter, β is scale parameter.

Step 2: Estimation of the cumulative probability

$$H(x) = p + (1-p)G(x) \tag{A3}$$

Where p is probability of no precipitation

Step 3: Transformation of the cumulative probability to the standard normal variable

$$Z = \begin{cases} -\left(W - \dfrac{C_0 + C_1 W + C_2 W^2}{1 + d_2 W + d_2 W^2 + d_3 W^3}\right) & 0 < H(x) \leq 0.5 \\ +\left(W - \dfrac{C_0 + C_1 W + C_2 W^2}{1 + d_2 W + d_2 W^2 + d_3 W^3}\right) & 0.5 < H(x) \leq 1 \end{cases} \quad \text{(A4)}$$

Where

$$W = \begin{cases} \sqrt{-2\,ln(H(x))} & 0 < H(x) \leq 0.5 \\ \sqrt{-2\,ln(1 - H(x))} & 0.5 < H(x) \leq 1 \end{cases}$$

And

$$C_0 = 2.515517, C_1 = 0.802853, C_2 = 0.010328$$

$$d_1 = 1.432788, d_2 = 0.189269, d_3 = 0.001308$$

Value Z is representative for SPI.

Appendix 2. Standardized Streamflow Index (SSI) calculation

The concept of SSI calculation is very similar to that of SPI calculation. Based on the empirical probability formula (Gringorten, 1963), we calculated the cumulative probability of streamflow for each month as follows:

$$\mathrm{H(x)} = \frac{i - 0.44}{n + 0.12} \tag{A5}$$

Where i is the rank of the observed streamflow from the smallest and n is the number of streamflow observations.

Then, we convert H(x) to a standard normal variable following equation (A4).

The SPI and SSI drought threshold are defined as their values smaller than -1.

585 **Appendix 3. Normalized satellite based SMAP soil moisture**

$$\theta_{SMAP,normal} = \left(\theta_{SMAP,raw} - \overline{\theta_{SMAP,raw}}\right) \times \frac{std(\theta_{in-situ})}{std(\theta_{SMAP,raw})} + \theta_{in-situ} \quad \text{(A6)}$$

586 Where $\theta_{SMAP,normal}$ is normalized SMAP soil moisture [m^3/ m^3], $\theta_{SMAP,raw}$ is raw SMAP soil moisture

587 [m^3/ m^3], $\theta_{in-situ}$ is *in-situ* soil moisture [m^3/ m^3]. $\bar{\theta}$ is the mean of θ, and std is standard deviation.

588

Appendix 4. Comparison of soil moisture delta changes measured at *in-situ* sites (MySMNet) with (a) SM9 soil moisture and (b) SM1 soil moisture.

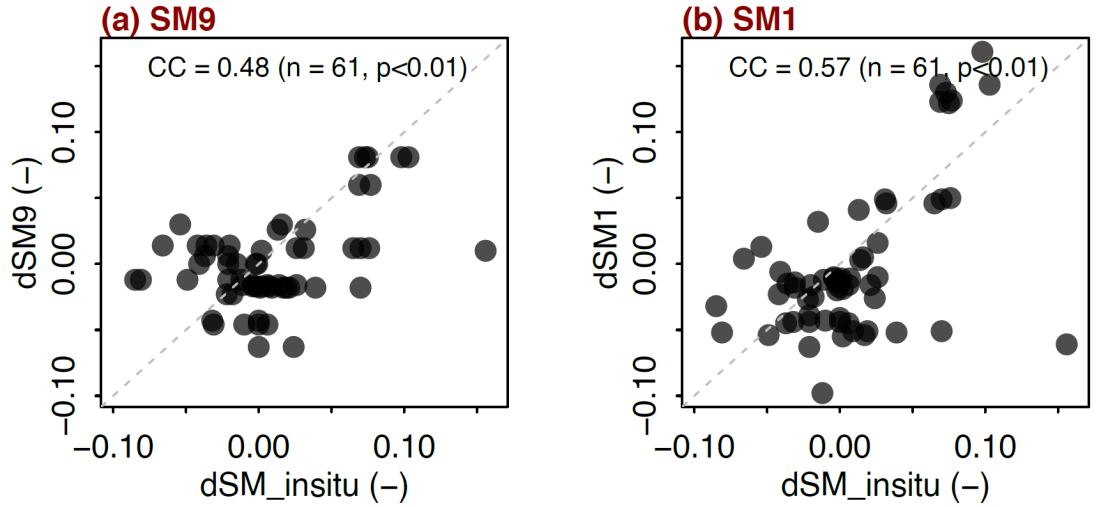

References

Abhishek, A., Das, N.N., Ines, A.V.M., Andreadis, K.M., Jayasinghe, S., Granger, S., Ellenburg, W.L., Dutta, R., Quyen, N.H., Markert, A.M., 2021. Evaluating the impacts of drought on rice productivity over Cambodia in the Lower Mekong Basin. Journal of Hydrology, 599: 126291.

Basist, A., Williams, C., 2020. Monitoring the Quantity of Water Flowing Through the Upper Mekong Basin Under Natural (Unimpeded) Conditions.

Binh, D.V., Kantoush, S.A., Sumi, T., Mai, N.P., Ngoc, T.A., Trung, L.V., An, T.D., 2021. Effects of riverbed incision on the hydrology of the Vietnamese Mekong Delta. Hydrological Processes, 35(2): e14030.

Bolten, J.D., Crow, W.T., 2012. Improved prediction of quasi‐global vegetation conditions using remotely‐sensed surface soil moisture. Geophysical Research Letters, 39(19).

Bolten, J.D., Crow, W.T., Zhan, X., Jackson, T.J., Reynolds, C.A., 2010. Evaluating the utility of remotely sensed soil moisture retrievals for operational agricultural drought monitoring. IEEE Journal of Selected Topics in Applied Earth Observations and Remote Sensing, 3(1): 57-66.

Bolten, J.D., Lakshmi, V., 2009. An evaluation of soil moisture retrievals using aircraft and satellite passive microwave observations during SMEX02. Journal of the Remote Sensing Society of Japan, 29(1): 293-300.

Bradford, J.B., Schlaepfer, D.R., Lauenroth, W.K., Palmquist, K.A., 2020. Robust ecological drought projections for drylands in the 21st century. Global change biology, 26(7): 3906-3919.

Chan, S.K., Bindlish, R., O'Neill, P.E., Njoku, E., Jackson, T., Colliander, A., Chen, F., Burgin, M., Dunbar, S., Piepmeier, J., 2016. Assessment of the SMAP passive soil moisture product. IEEE Transactions on Geoscience and Remote Sensing, 54(8): 4994-5007.

Christian, J.I., Basara, J.B., Otkin, J.A., Hunt, E.D., Wakefield, R.A., Flanagan, P.X., Xiao, X., 2019. A methodology for flash drought identification: Application of flash drought frequency across the United States. Journal of Hydrometeorology, 20(5): 833-846.

615 Colliander, A., Cosh, M.H., Kelly, V.R., Kraatz, S., Bourgeau‐Chavez, L., Siqueira, P., Roy, A., Konings, A.G.,
616 Holtzman, N., Misra, S., 2020. SMAP detects soil moisture under temperate forest canopies. Geophysical
617 Research Letters, 47(19): e2020GL089697.

618 Colliander, A., Jackson, T.J., Bindlish, R., Chan, S., Das, N., Kim, S.B., Cosh, M.H., Dunbar, R.S., Dang, L., Pashaian,
619 L., 2017. Validation of SMAP surface soil moisture products with core validation sites. Remote sensing of
620 environment, 191: 215-231.

621 Crausbay, S.D., Ramirez, A.R., Carter, S.L., Cross, M.S., Hall, K.R., Bathke, D.J., Betancourt, J.L., Colt, S., Cravens,
622 A.E., Dalton, M.S., Dunham, J.B., Hay, L.E., Hayes, M.J., McEvoy, J., McNutt, C.A., Moritz, M.A., Nislow,
623 K.H., Raheem, N., Sanford, T., 2018. Defining Ecological Drought for the Twenty-First Century. Bulletin of
624 the American Meteorological Society, 98(12): 2543-2550. DOI:10.1175/BAMS-D-16-0292.1

625 Dandridge, C., Fang, B., Lakshmi, V., 2020. Downscaling of SMAP Soil Moisture in the Lower Mekong River Basin.
626 Water, 12(1): 56.

627 Doan, V.B., Kantoush, S.A., Saber, M., Mai, N.P., Maskey, S., Phong, D.T., Sumi, T., 2020. Long-term alterations of
628 flow regimes of the Mekong River and adaptation strategies for the Vietnamese Mekong Delta. Journal of
629 Hydrology: Regional Studies, 32: 100742.

630 Dong, Z., Liu, H., Hu, H., Khan, M.Y.A., Wen, J., Chen, L., Tian, F., 2022. Future projection of seasonal drought
631 characteristics using CMIP6 in the Lancang-Mekong River Basin. Journal of Hydrology, 610: 127815.

632 Dorigo, W., Himmelbauer, I., Aberer, D., Schremmer, L., Petrakovic, I., Zappa, L., Preimesberger, W., Xaver, A.,
633 Annor, F., Ardö, J., 2021. The International Soil Moisture Network: serving Earth system science for over a
634 decade. Hydrology and earth system sciences, 25(11): 5749-5804.

635 Draper, C.S., Walker, J.P., Steinle, P.J., De Jeu, R.A.M., Holmes, T.R.H., 2009. An evaluation of AMSR–E derived
636 soil moisture over Australia. Remote Sensing of Environment, 113(4): 703-710.

637 Elhag, K.M., Zhang, W., 2018. Monitoring and assessment of drought focused on its impact on sorghum yield over
638 Sudan by using meteorological drought indices for the period 2001–2011. Remote Sensing, 10(8): 1231.

639 Entekhabi, D., Njoku, E.G., O'Neill, P.E., Kellogg, K.H., Crow, W.T., Edelstein, W.N., Entin, J.K., Goodman, S.D.,
640 Jackson, T.J., Johnson, J., 2010. The soil moisture active passive (SMAP) mission. Proceedings of the IEEE,
641 98(5): 704-716.

642 Fang, B., Lakshmi, V., Bindlish, R., Jackson, T.J., Cosh, M., Basara, J., 2013. Passive microwave soil moisture
643 downscaling using vegetation index and skin surface temperature. Vadose Zone Journal, 12(3).

644 Fang, B., Lakshmi, V., Bindlish, R., Jackson, T.J., Liu, P.-W., 2020. Evaluation and validation of a high spatial
645 resolution satellite soil moisture product over the Continental United States. Journal of Hydrology, 588:
646 125043.

647 Fang, B., Lakshmi, V., Cosh, M., Liu, P.W., Bindlish, R., Jackson, T.J., 2022. A global 1-km downscaled SMAP soil
648 moisture product based on thermal inertia theory. Vadose Zone Journal: e20182.

649 Farahmand, A., AghaKouchak, A., 2015. A generalized framework for deriving nonparametric standardized drought
650 indicators. Advances in Water Resources, 76: 140-145.

651 Frappart, F., Seoane, L., Ramillien, G., 2013. Validation of GRACE-derived terrestrial water storage from a regional
652 approach over South America. Remote Sensing of Environment, 137: 69-83.

653 Funk, C., Peterson, P., Landsfeld, M., Pedreros, D., Verdin, J., Shukla, S., Husak, G., Rowland, J., Harrison, L., Hoell,
654 A., 2015. The climate hazards infrared precipitation with stations—a new environmental record for
655 monitoring extremes. Scientific data, 2: 150066.

656 Gringorten, I.I., 1963. A plotting rule for extreme probability paper. Journal of Geophysical Research, 68(3): 813-
657 814.

658 Gudmundsson, L., Boulange, J., Do, H.X., Gosling, S.N., Grillakis, M.G., Koutroulis, A.G., Leonard, M., Liu, J.,
659 Müller Schmied, H., Papadimitriou, L., 2021. Globally observed trends in mean and extreme river flow
660 attributed to climate change. Science, 371(6534): 1159-1162.

661 Guo, H., Bao, A., Liu, T., Ndayisaba, F., He, D., Kurban, A., De Maeyer, P., 2017. Meteorological drought analysis
662 in the Lower Mekong Basin using satellite-based long-term CHIRPS product. Sustainability, 9(6): 901.

Ha, T.V., Huth, J., Bachofer, F., Kuenzer, C., 2022. A Review of Earth Observation-Based Drought Studies in Southeast Asia. Remote Sensing, 14(15): 3763.

Hou, A.Y., Kakar, R.K., Neeck, S., Azarbarzin, A.A., Kummerow, C.D., Kojima, M., Oki, R., Nakamura, K., Iguchi, T., 2014. The global precipitation measurement mission. Bulletin of the American Meteorological Society, 95(5): 701-722.

Hu, C., Xia, J., She, D., Li, L., Song, Z., Hong, S., 2021. A new framework for the identification of flash drought: Multivariable and probabilistic statistic perspectives: Identification of flash drought. International Journal of Climatology, 41(13): 5862-5878.

Huffman, G.J., 2016. The Transition in Multi-Satellite Products from TRMM to GPM (TMPA to IMERG), NASA/GSFC Code.

Huffman, G.J., Bolvin, D.T., Braithwaite, D., Hsu, K.-L., Joyce, R.J., Kidd, C., Nelkin, E.J., Sorooshian, S., Stocker, E.F., Tan, J., 2020. Integrated multi-satellite retrievals for the Global Precipitation Measurement (GPM) mission (IMERG), Satellite precipitation measurement. Springer, Cham, pp. 343-353.

Jones, J.W., Hoogenboom, G., Porter, C.H., Boote, K.J., Batchelor, W.D., Hunt, L.A., Wilkens, P.W., Singh, U., Gijsman, A.J., Ritchie, J.T., 2003. The DSSAT cropping system model. European journal of agronomy, 18(3-4): 235-265.

Kang, C.S., Kanniah, K.D., Kerr, Y.H., 2019. Calibration of SMOS soil moisture retrieval algorithm: A case of tropical site in Malaysia. IEEE Transactions on Geoscience and Remote Sensing, 57(6): 3827-3839.

Kang, H., Sridhar, V., Mainuddin, M., Trung, L.D., 2021. Future rice farming threatened by drought in the Lower Mekong Basin. Scientific reports, 11(1): 1-15.

Kansara, P., Lakshmi, V., 2021. Estimation of land-cover linkage to trends in hydrological variables of river basins in the Indian sub-continent using satellite observation and model outputs. Journal of Hydrology, 603: 126997.

Kantoush, S., Van Binh, D., Sumi, T., Trung, L.V., 2017. Impact of upstream hydropower dams and climate change on hydrodynamics of Vietnamese Mekong Delta. 土木学会論文集 B1 (水工学), 73(4): I_109-I_114.

687 Keovilignavong, O., Nguyen, T.H., Hirsch, P., 2021. Reviewing the causes of Mekong drought before and during
688 2019–20. International Journal of Water Resources Development: 1-21.

689 Kerr, Y.H., Waldteufel, P., Wigneron, J.P., Martinuzzi, J., Font, J., Berger, M., 2001. Soil moisture retrieval from
690 space: The Soil Moisture and Ocean Salinity (SMOS) mission. IEEE transactions on Geoscience and remote
691 sensing, 39(8): 1729-1735.

692 Kim, H., Wigneron, J.-P., Kumar, S., Dong, J., Wagner, W., Cosh, M.H., Bosch, D.D., Collins, C.H., Starks, P.J.,
693 Seyfried, M., 2020. Global scale error assessments of soil moisture estimates from microwave-based active
694 and passive satellites and land surface models over forest and mixed irrigated/dryland agriculture regions.
695 Remote Sensing of Environment, 251: 112052.

696 Kim, S., Parinussa, R.M., Liu, Y.Y., Johnson, F.M., Sharma, A., 2015. A framework for combining multiple soil
697 moisture retrievals based on maximizing temporal correlation. Geophysical Research Letters, 42(16): 6662-
698 6670.

699 Lakshmi, V., 2013. Remote sensing of soil moisture. ISRN Soil Science, 2013.

700 Lakshmi, V., Fayne, J., Bolten, J., 2018. A comparative study of available water in the major river basins of the world.
701 Journal of Hydrology, 567: 510-532.

702 Le, M.-H., Kim, H., Moon, H., Zhang, R., Lakshmi, V., Nguyen, L.-B., 2020a. Assessment of drought conditions over
703 Vietnam using standardized precipitation evapotranspiration index, MERRA-2 re-analysis, and dynamic land
704 cover. Journal of Hydrology: Regional Studies, 32: 100767. DOI:https://doi.org/10.1016/j.ejrh.2020.100767

705 Le, M.-H., Lakshmi, V., Bolten, J., Bui, D.D., 2020b. Adequacy of Satellite-derived Precipitation Estimate for
706 Hydrological Modeling in Vietnam Basins. Journal of Hydrology, 586: 124820.
707 DOI:https://doi.org/10.1016/j.jhydrol.2020.124820

708 Le, M.-H., Nguyen, B.Q., Pham, H.T., Patil, A., Do, H.X., Ramsankaran, R., Bolten, J.D., Lakshmi, V., 2022.
709 Assimilation of SMAP Products for Improving Streamflow Simulations over Tropical Climate
710 Region—Is Spatial Information More Important Than Temporal Information? Remote Sensing, 14(7).
711 DOI:10.3390/rs14071607

712 Le, P.V.V., Phan‐Van, T., Mai, K.V., Tran, D.Q., 2019. Space‐time variability of drought over Vietnam.
713 International Journal of Climatology.

714 Li, Y., Lu, H., Yang, K., Wang, W., Tang, Q., Khem, S., Yang, F., Huang, Y., 2021. Meteorological and hydrological
715 droughts in Mekong River Basin and surrounding areas under climate change. Journal of Hydrology:
716 Regional Studies, 36: 100873.

717 McKee, T.B., Doesken, N.J., Kleist, J., 1993. The relationship of drought frequency and duration to time scales,
718 Proceedings of the 8th Conference on Applied Climatology. Boston, pp. 179-183.

719 Mohammed, I.N., Bolten, J.D., Srinivasan, R., Lakshmi, V., 2018a. Improved Hydrological Decision Support System
720 for the Lower Mekong River Basin Using Satellite-Based Earth Observations. Remote sensing, 10(6).

721 Mohammed, I.N., Bolten, J.D., Srinivasan, R., Lakshmi, V., 2018b. Satellite observations and modeling to understand
722 the Lower Mekong River Basin streamflow variability. Journal of hydrology, 564: 559-573.

723 Mohammed, I.N., Bolten, J.D., Srinivasan, R., Meechaiya, C., Spruce, J.P., Lakshmi, V., 2018c. Ground and satellite
724 based observation datasets for the Lower Mekong River Basin. Data in brief, 21: 2020-2027.

725 Mondal, A., Le, M.-H., Lakshmi, V., 2022. Land use, climate, and water change in the Vietnamese Mekong Delta
726 (VMD) using earth observation and hydrological modeling. Journal of Hydrology: Regional Studies, 42:
727 101132.

728 MRC, 2003. State of the Basin Report, State of the Basin Report Executive Summary, Phnom Penh, Camboda.

729 MRC, 2019. Annual Report 2019, Part 1, Progress and Achievements. Accessed 16 Apr 2021.
730 https://www.mrcmekong.org/assets/Publications/AR2019-Part-1.pdf.

731 Naeimi, V., Leinenkugel, P., Sabel, D., Wagner, W., Apel, H., Kuenzer, C., 2013. Evaluation of soil moisture retrieval
732 from the ERS and Metop scatterometers in the lower Mekong Basin. Remote Sensing, 5(4): 1603-1623.

733 Park, E., Loc, H.H., Van Binh, D., Kantoush, S., 2022. The worst 2020 saline water intrusion disaster of the past
734 century in the Mekong Delta: Impacts, causes, and management implications. Ambio, 51(3): 691-699.

Pham, H.T., Marshall, L., Johnson, F., 2021. Daily time series of river water levels derived from a seasonal linear model using multisource satellite products under uncertainty. Journal of Hydrology, 602: 126783.

Pham, H.T., Marshall, L., Johnson, F., Sharma, A., 2018. Deriving daily water levels from satellite altimetry and land surface temperature for sparsely gauged catchments: A case study for the Mekong River. Remote Sensing of Environment, 212: 31-46.

Rodell, M., Velicogna, I., Famiglietti, J.S., 2009. Satellite-based estimates of groundwater depletion in India. Nature, 460(7258): 999-1002.

Sheffield, J., Wood, E.F., Pan, M., Beck, H., Coccia, G., Serrat‐Capdevila, A., Verbist, K., 2018. Satellite Remote Sensing for Water Resources Management: Potential for Supporting Sustainable Development in Data‐Poor Regions. Water Resources Research, 54(12): 9724-9758.

Son, B., Park, S., Im, J., Park, S., Ke, Y., Quackenbush, L.J., 2021. A new drought monitoring approach: Vector Projection Analysis (VPA). Remote Sensing of Environment, 252: 112145.

Son, N.T., Chen, C.F., Chen, C.R., Chang, L.Y., Minh, V.Q., 2012. Monitoring agricultural drought in the Lower Mekong Basin using MODIS NDVI and land surface temperature data. International Journal of Applied Earth Observation and Geoinformation, 18: 417-427.

Syed, T.H., Famiglietti, J.S., Rodell, M., Chen, J., Wilson, C.R., 2008. Analysis of terrestrial water storage changes from GRACE and GLDAS. Water Resources Research, 44(2).

Tallaksen, L., 2000. Streamflow drought frequency analysis, Drought and drought mitigation in Europe. Springer, pp. 103-117.

Tapley, B.D., Bettadpur, S., Watkins, M., Reigber, C., 2004. The gravity recovery and climate experiment: Mission overview and early results. Geophysical Research Letters, 31(9).

Telesca, L., Lovallo, M., Lopez-Moreno, I., Vicente-Serrano, S., 2012. Investigation of scaling properties in monthly streamflow and Standardized Streamflow Index (SSI) time series in the Ebro basin (Spain). Physica A: Statistical Mechanics and its Applications, 391(4): 1662-1678.

759 Thiessen, A.H., 1911. Precipitation averages for large areas. Monthly weather review, 39(7): 1082-1089.

760 Thilakarathne, M., Sridhar, V., 2017. Characterization of future drought conditions in the Lower Mekong River Basin.
761 Weather and Climate Extremes, 17: 47-58.

762 Thomas, B.F., Famiglietti, J.S., Landerer, F.W., Wiese, D.N., Molotch, N.P., Argus, D.F., 2017. GRACE groundwater
763 drought index: Evaluation of California Central Valley groundwater drought. Remote Sensing of
764 Environment, 198: 384-392.

765 Thornthwaite, C.W., 1947. Climate and moisture conservation. Annals of the Association of American Geographers,
766 37(2): 87-100.

767 Tran, D.A., Tsujimura, M., Ha, N.T., Van Binh, D., Dang, T.D., Doan, Q.-V., Bui, D.T., Ngoc, T.A., Thuc, P.T.B.,
768 Pham, T.D., 2021. Evaluating the predictive power of different machine learning algorithms for groundwater
769 salinity prediction of multi-layer coastal aquifers in the Mekong Delta, Vietnam. Ecological Indicators, 127:
770 107790.

771 Tran, T.V., Tran, D.X., Myint, S.W., Latorre-Carmona, P., Ho, D.D., Tran, P.H., Dao, H.N., 2019. Assessing
772 Spatiotemporal Drought Dynamics and Its Related Environmental Issues in the Mekong River Delta. Remote
773 Sensing, 11(23): 2742.

774 Vörösmarty, C.J., McIntyre, P.B., Gessner, M.O., Dudgeon, D., Prusevich, A., Green, P., Glidden, S., Bunn, S.E.,
775 Sullivan, C.A., Liermann, C.R., 2010. Global threats to human water security and river biodiversity. nature,
776 467(7315): 555-561.

777 Voss, K.A., Famiglietti, J.S., Lo, M., De Linage, C., Rodell, M., Swenson, S.C., 2013. Groundwater depletion in the
778 Middle East from GRACE with implications for transboundary water management in the Tigris‐
779 Euphrates‐Western Iran region. Water resources research, 49(2): 904-914.

780 Wang, F., Wang, Z., Yang, H., Di, D., Zhao, Y., Liang, Q., 2020. Utilizing GRACE-based groundwater drought index
781 for drought characterization and teleconnection factors analysis in the North China Plain. Journal of
782 Hydrology, 585: 124849.

West, H., Quinn, N., Horswell, M., 2019. Remote sensing for drought monitoring & impact assessment: Progress, past challenges and future opportunities. Remote Sensing of Environment, 232: 111291.

Wilhite, D.A., 2000. Drought as a natural hazard: concepts and definitions.

Wilhite, D.A., Glantz, M.H., 1985. Understanding: the drought phenomenon: the role of definitions. Water international, 10(3): 111-120.

WMO, GWP, 2016. Handbook of drought indicators and indices.

Zhang, B., Zhang, L., Guo, H., Leinenkugel, P., Zhou, Y., Li, L., Shen, Q., 2014. Drought impact on vegetation productivity in the Lower Mekong Basin. International journal of remote sensing, 35(8): 2835-2856.

Zhang, L., Jiao, W., Zhang, H., Huang, C., Tong, Q., 2017. Studying drought phenomena in the Continental United States in 2011 and 2012 using various drought indices. Remote sensing of environment, 190: 96-106.

Zhang, X., Qu, Y., Ma, M., Liu, H., Su, Z., Lv, J., Peng, J., Leng, G., He, X., Di, C., 2020. Satellite-Based Operational Real-Time Drought Monitoring in the Transboundary Lancang–Mekong River Basin. Remote Sensing, 12(3): 376.

Zhongming, Z., Linong, L., Xiaona, Y., Wangqiang, Z., Wei, L., 2021. AR6 Climate Change 2021: The Physical Science Basis.

Conflicts of Interest

The authors declare no conflict of interest.

802 **List of Tables**

List of Figures

9 (top) mapping soil moisture variability at high spatial resolution and (bottom) boxplot of soil moisture distribution for catchment I.14 for the 2015-16 water year

10 Variability of precipitation, soil moisture and stream flowrunoff in (a) G.9, (b) Banyen, (c) Kh.28a, (d) G.8, and (e) I.14 for the 2015-16 water year.

11 Comparison of (a) anomalies precipitation, (b) runoff, and (c), (d), (e) relationship between Standardized Streamflow Index (SSI) and Standardized Precipitation Index (SPI). The dash red lines in (a) and (b) represent normal value of the anomalies time series for the 2015-16 water year. The Max CC at Lag 0, 1, 2 denote catchments (black dots) having maximum correlation coefficient between SPI and SSI at lag 0, lag1, and lag2 of SPI for the 2015-16, respectively. The dots with circles are statistical significant locations at significant level 0.1 for two-sided t-test. The coordinates of catchment locations are taken as the centroids of catchment boundaries. The underlying TWSA maps in (c), (d), (e) are the mean TWSA during the 2015-16 water year extracted from GRACE.

12 Monthly changes for the 2015-16 water year in standardized streamflow index (SSI), standardized precipitation index (SPI) and soil moisture for catchment in (a) G.9; (b) Banyen; (c) Kh.28A; (d) G.8, and (e) I.14. The panel (f) presents cross correlation between monthly changes in SPI, SM9, SM1 and monthly changes in SSI for each catchment in (a), (b), (c), (d), and (e).

852 Table 1 Several studies on remote sensing-based drought monitoring in the LMRB

Study	Remote sensing datasets /spatial resolutions	Drought types	Methods and key findings
(Abhishek et al., 2021)	CHIRPS precipitation / 5 km SMAP soil moisture / ~ 30 km	Meteorological drought, Agricultural drought	A regional drought study over Cambodia was carried on for the period 1981-2019. CHIRPS precipitation has been forced to a hydrological model and SMAP soil moisture has been used to validate hydrological model-based soil moisture. Hydrological model-based drought monitoring with remote sensing forcing inputs could reasonably capture meteorological and agricultural drought and interannual variability of rice yields.
(Zhang et al., 2020)	TRMM precipitation/ 25 km	Hydrological drought	This study proposed a near-real time drought monitoring system forcing by bias-corrected near-real time satellite precipitation. The system was validated during 2005-2014, successfully reproducing two drought events in 2004/05 and 2009/10.
(Tran et al., 2019)	MODIS LST/ 1 km MODIS EVI / 0.5 km MODIS ET and PET/0.5 km	Agricultural drought	This study proposed an Enhanced Drought Severity Index (EDSI) derived from ET, PET, LST, and EVI. The EDSI was applied to analyze spatio-temporal drought trends in the Vietnamese Mekong Delta from 2001-2018, demonstrating more serve drought in the coastal regions.
(Guo et al., 2017)	CHIRPS precipitation / 5 km	Meteorological drought	The Standardized Precipitation Index (SPI) at various time scales (1-12 month) was calculated over LMRB using CHIRPS dataset from 1981-2016. The LMRB experienced four severe drought episodes with the longest period in 1991-1994 and the driest period in 2015-16.

(Zhang et al., 2014)	MODIS GPP and NPP/ 1km	Agricultural drought	The changes in vegetation productivity over the LMRB were assessed during 2000-2011. This study identified the impacts of severe droughts in 2005 and 2010 on vegetation productivity, with more pronounced impacts for Cambodia and Laos.
(Son et al., 2012)	MODIS NDVI/ 5 km MODIS LST/ 5 km AMSR-E soil moisture/ 25 km TRMM precipitation/ 25 km	Agricultural drought	This study proposed Temperature Vegetation Dryness Index (TVDI) index utilizing NDVI and LST datasets. The AMSR-E and TRMM were used to cross-validate TVDI. The TDVI was sensitive the most to soil moisture stress. Consequently, this study used TVDI to investigate spatial drought condition in the LMRB during 2002-2010 dry seasons, observing a large serve drought for the 2003-2006 dry seasons.

853 Note: 'LST' Land Surface Temperature; 'EVI' Enhanced Vegetation Index; 'ET' Evapotranspiration; 'PET' Potential
854 evapotranspiration; 'GPP' Gross Primary Productivity; 'NPP' Net Primary Productivity

855

Table 2 List of streamflow gages and catchments used in this study

Station name	River system	Stream	Long. (°)	Lat. (°)	Collection time	Dominant land cover	Area (km²)	Sources
Kh.89	Khong	Nam Mae Chan	99.8625	20.157	1993-2019	shrublands	248	rid
M.145	Mun	Lam Phra Phloeng	101.687	14.49	1990-2019	croplands	335	rid
G.9*	**Name Mae Kok**	**Mae Suai**	**99.5075**	**19.748**	**1999-2019**	**shrublands**	**386**	**rid**
Krongbuk	Srepok	Krongbuk	108.376	12.772	1977-2019	shrublands	503	vmha
Kh.61	Khong	Loei	101.682	17.129	1993-2019	no dominant	549	rid
Banyen*	**Nam Mua**	**Nam Rom**	**103.014**	**21.274**	**1976-2019**	**shrublands**	**638**	**vmha**
Kh.72	Khong	Nam Mae Chan	99.8606	20.217	1993-2019	shrublands	667	rid
M.89	Mun	Lam Takhong	101.417	14.694	1970-2019	no dominant	713	rid
Kh.28A*	**Khong**	**Loei**	**101.774**	**17.309**	**1993-2019**	**no dominant**	**1271**	**rid**
E.32A	Chi	Chi	101.712	15.911	1967-2019	no dominant	2867	rid
G.8*	**Name Mae Kok**	**Nam Mae Lao**	**99.7531**	**19.792**	**1994-2019**	**no dominant**	**2909**	**rid**
Kh.58A	Khong	Loei	101.738	17.493	1990-2019	shrublands	3093	rid
Giangson	Srepok	Krong Ana	108.183	12.51	1978-2019	no dominant	3100	vmha
E.5	Chi	Chi	101.817	15.769	1958-2019	no dominant	4207	rid
I.14*	**Khong**	**Mae Nam Ing**	**100.204**	**19.832**	**1993-2019**	**no dominant**	**6266**	**rid**
E.9	Chi	Chi	102.574	16.096	1967-2019	croplands	10878	rid

Note: Bold and asterisk are selected catchments for soil moisture spatial analysis. Land cover data was extracted from MODIS Land cover MCD12Q1 V6 in the year 2016. Dominant land cover was assigned for a land cover type as it accounts for more than 50% of the total area. If there are no land cover type accounts for than 50% of the total area, 'no dominant' was assigned.

861 Table 3 List of data used in this study

Measurements	Data type	Description	Spatial/ temporal resolutions	Study period	Sources
In-situ	Stream gauge	Sixteen stations	monthly/ -	Varied	RID*, VMHA**
	Soil moisture	Two networks	daily/ -	Varied	ISMN***
Earth Observations	Precipitation	GPM IMERG Final	monthly/ 0.1°	2001-2020	(Hou et al., 2014)
	Soil moisture	SMAP	daily/ 0.09°	2015-16	(Entekhabi et al., 2010)
		Downscaled SMAP	daily/ 0.01°	2015-16	(Fang et al., 2022)
	Terrestrial	GRACE RL06	monthly/ 0.1°	2002-2020	(Syed et al., 2008)

862 Note: * Royal Irrigation Department (RID); **Vietnam Meteorological and Hydrological Administration (VMHA); ***
863 International Soil Moisture Network (ISMN) .

864

865 Table 4 Correlation between P, S, Q for all 16 small catchments listed in Table 2

Station	Available_{SM9}	Available_{SM1}	CC_{RP}	CC_{RSM9}	CC_{PSM9}	CC_{RSM1}	CC_{PSM1}	CC_{SM9SM1}
Kh.89	97.0	99.6	0.748	0.758	0.948	0.751	0.918	0.985
M.145	97.8	97.4	0.412	0.624	0.917	0.337	0.800	0.842
G.9*	99.4	100.0	0.836	0.878	0.944	0.900	0.934	0.978
Krongbuk	99.5	100.0	0.369	0.292	0.813	0.240	0.730	0.942
Kh.61	99.4	97.1	0.690	0.633	0.929	0.671	0.869	0.948
Banyen*	99.6	100.0	0.712	0.149	0.436	0.326	0.259	0.815
Kh.72	97.8	99.9	0.705	0.744	0.949	0.751	0.915	0.985
M.89	97.5	97.2	0.673	0.645	0.867	0.218	0.670	0.817
Kh.28A*	98.1	96.8	0.639	0.627	0.937	0.659	0.872	0.951
E.32A	98.6	92.7	0.759	0.735	0.913	0.560	0.795	0.897
G.8*	98.5	99.5	0.548	0.530	0.946	0.542	0.937	0.988
Kh.58A	98.7	94.0	0.646	0.677	0.946	0.687	0.875	0.957
Giangson	98.6	99.7	0.682	0.837	0.762	0.735	0.704	0.959
E.5	98.9	92.5	0.693	0.665	0.917	0.402	0.767	0.872
I.14*	98.9	98.6	0.641	0.708	0.895	0.714	0.876	0.990
E.9	99.3	92.4	0.589	0.709	0.917	0.515	0.808	0.908
Median	98.6	97.3	0.678	0.671	0.917	0.610	0.839	0.950

866 Note: Available_{SM9}, Available_{SM1} are the percentage of monthly available soil moisture from SMAP 9km and SMAP 1km during
867 the study period 2015-16, respectively. CC stands for correlation coefficient. Subscript of R, P, SM9, SM1 denote runoff,
868 precipitation, SMAP 9km, and SMAP 1km, respectively. The symbol, for example, $\boldsymbol{CC_{RP}}$ indicates correlation between Runoff
869 and Precipitation.

Table 5 Description of drought characteristics for Standardized Streamflow Index (SSI) and Standardized Precipitation Index (SPI) for all 16 small catchments. Absolute values have been used for drought severity. One drought episode is counted as at least two consecutive months are under the drought threshold. The drought threshold for SPI and SSI are -1.

Station names	Drought indices	Started date/ Ended date	No. drought episodes	Drought duration	Drought severity
Kh.89	SPI	03/16-04/16	1	2	1.78
	SSI	10/15-12/15	1	8	1.82
M.145	SPI	02/16-14/16	1	3	1.72
	SSI	12/15-06/16	1	7	1.73
G.9	SPI	03/16-04/16	1	2	1.75
	SSI	10/15-05/16	2	5	1.52
Krongbuk	SPI	03/16-04/16	1	2	1.42
	SSI	10/15-03/16	2	4	1.82
Kh.61	SPI	02/16-03/16	1	2	1.75
	SSI	10/15-12/15	2	2.5	1.66
Banyen	SPI	-	-	-	-
	SSI	-	-	-	-
Kh.72	SPI	03/16-04/16	1	2	1.50
	SSI	10/15-06/16	2	5.5	1.35
M.89	SPI	02/16-04/16	1	3	1.66
	SSI	10/15-09/16	1	12	1.72
Kh.28A	SPI	02/16-03/16	1	2	1.69
	SSI	12/15-06/16	1	7	1.73
E.32A	SPI	02/16-03/16	1	2	2.23
	SSI	11/15-03/16	1	5	2.22
G.8	SPI	03/16-04/16	1	2	1.66
	SSI	10/15-12/15	2	5.5	1.69
Kh.58A	SPI	02/16-03/16	1	2	1.66
	SSI	-	-	-	-
Giangson	SPI	03/16-04/16	1	2	1.50
	SSI	10/15-11/15	1	2	1.15
E.5	SPI	02/16-03/16	1	2	2.35
	SSI	03/16-05/16	1	3	1.97
I.14	SPI	03/16-04/16	1	2	1.75
	SSI	10/15-03/16	1	6	1.51
E.9	SPI	02/16-03/16	1	2	2.30
	SSI	11/15-01/16	1	3	0.96

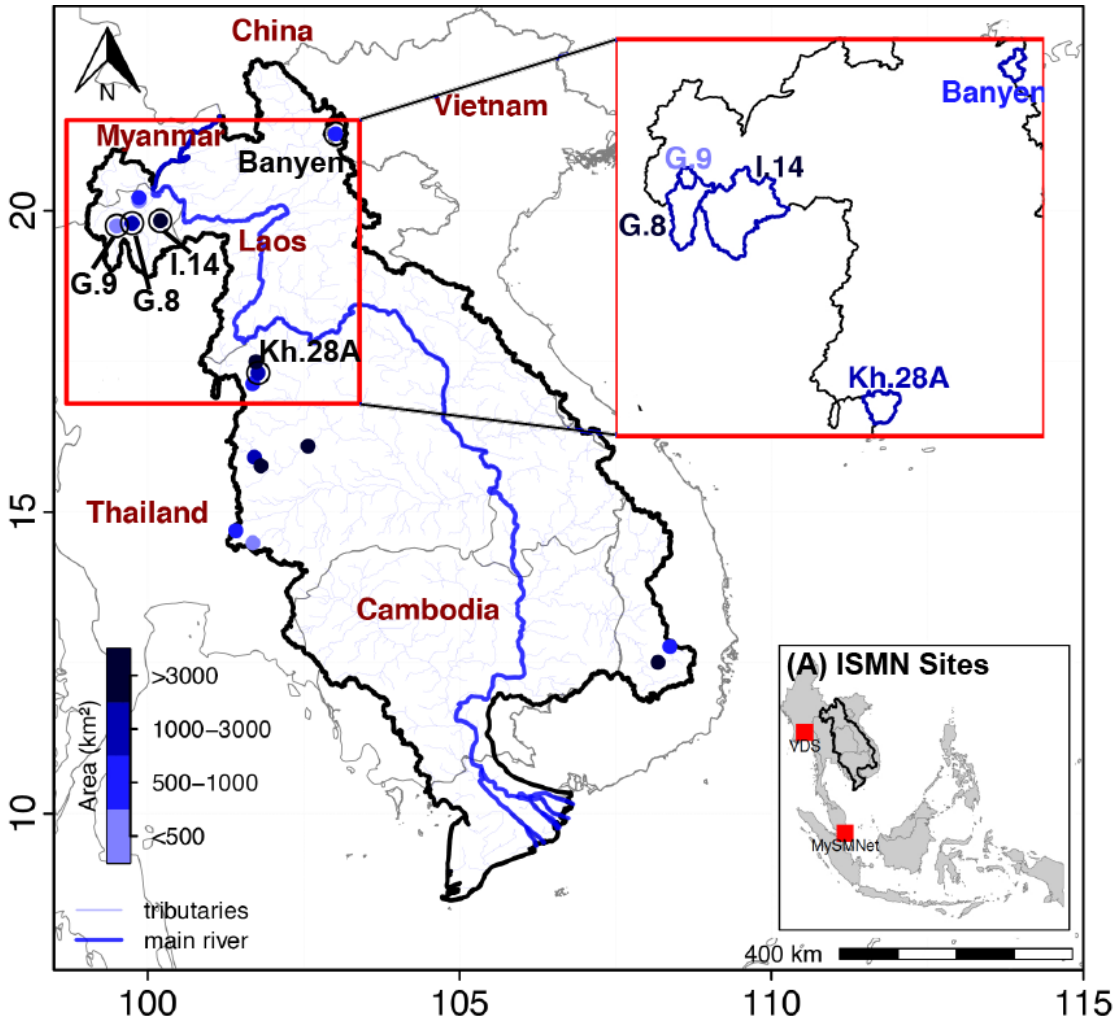

Figure 1 Locations of stream gauges (dots) in the Lower Mekong River basin (black dashed catchment boundary). The circles represent soil moisture stream gauge locations for spatial analysis, while the inlet panel shows catchment boundaries. In panel A, the red rectangles denote locations of two *in-situ* soil moisture networks from the International Soil Moisture Network (ISMN) in the Southeast Asia region.

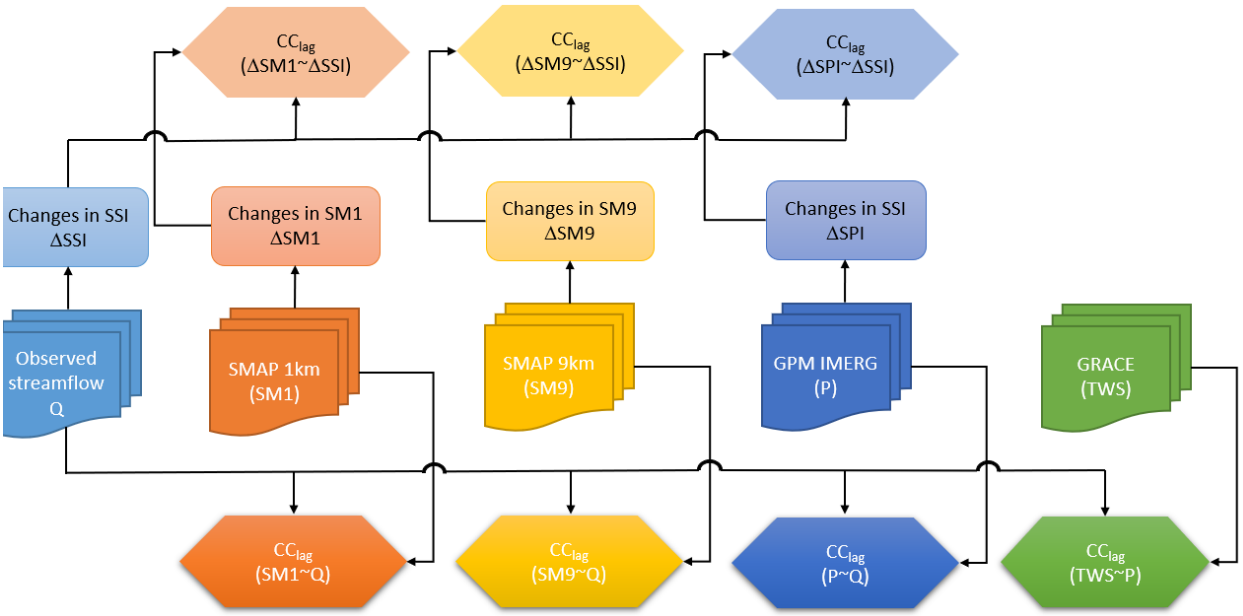

Figure 2 An overview of the flow of the study. CC_{lag} implies cross-correlation analysis between two variables.

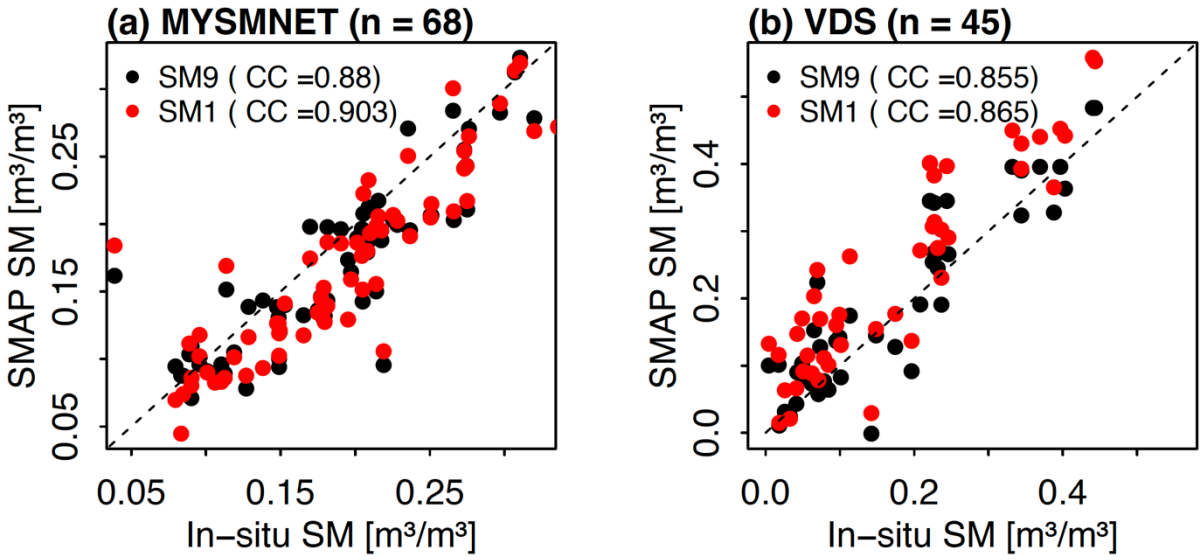

883

884 Figure 3 Inter-comparison between SMAP 9km soil moisture (SM9) and downscaled SMAP 1km soil moisture (SM1)
885 against *in-situ* soil moisture in (a) MySMNet and (b) VDS. Values in blankets denote spearman correlation coefficient
886 between each SMAP soil moisture product with *in-situ* soil moisture dataset.

887

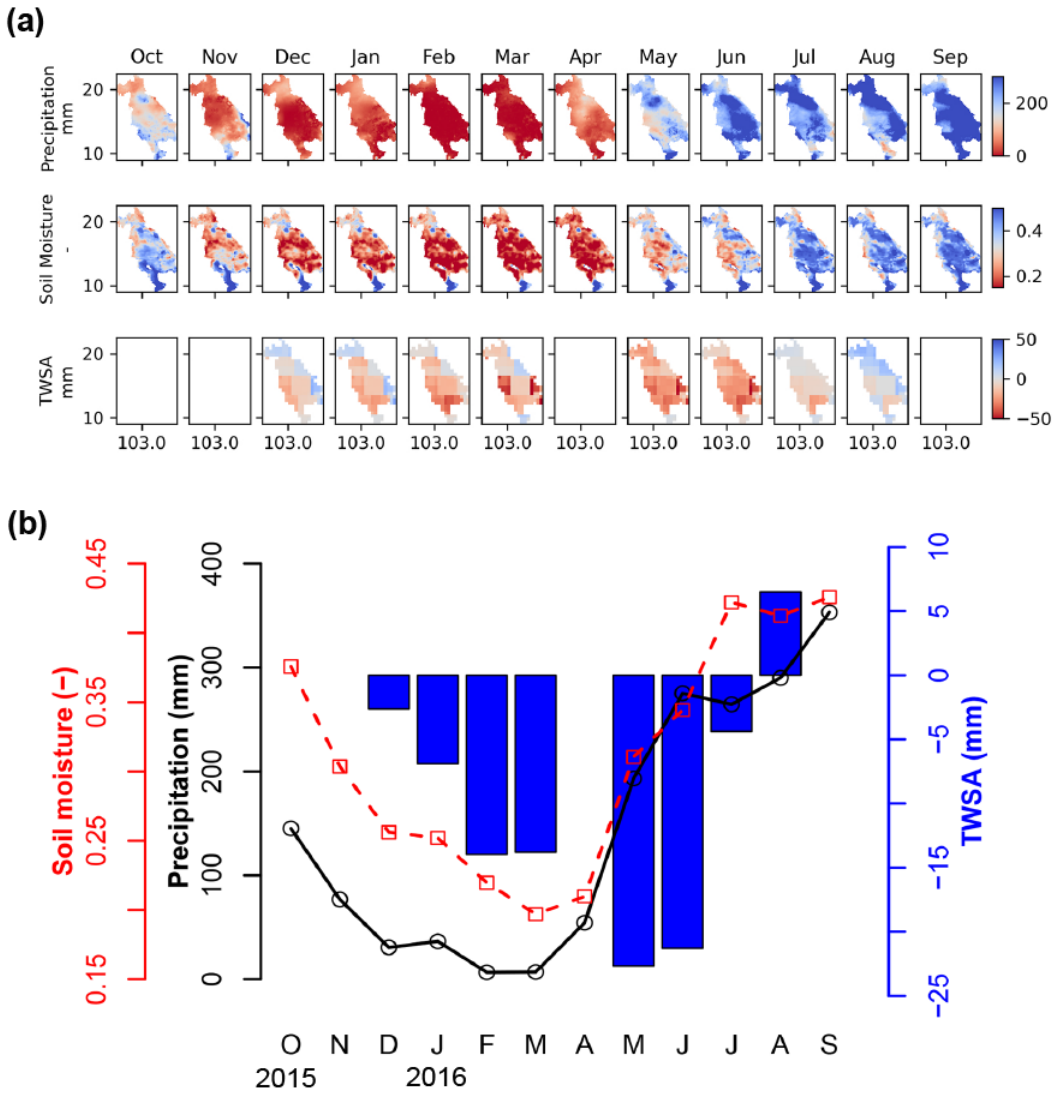

888

889 Figure 4 (a) Variability of precipitation, soil moisture and total water in the Lower Mekong River Basin for the 2015-16 water year
890 (b) time series of basin averaged variation of precipitation (black line), soil moisture (dash red line) and terrestrial water storage
891 anomalies (blue bar) for the 2015-16 water year in the Lower Mekong River Basin.

892

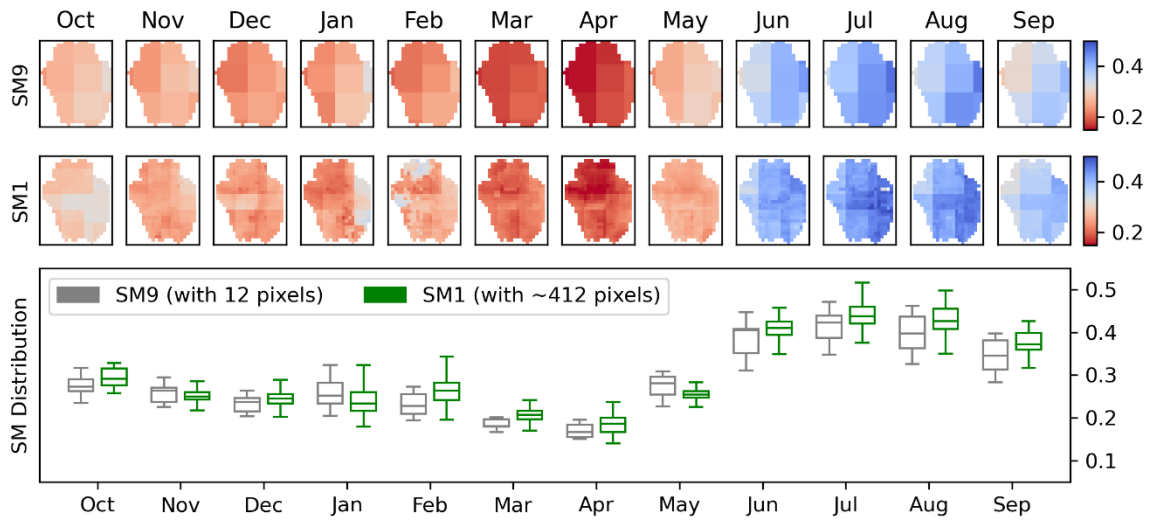

893

894 Figure 5 (top) mapping soil moisture variability at high spatial resolution and (bottom) boxplot of soil moisture distribution for

895 catchment G.9 for the 2015-16 water year.

896

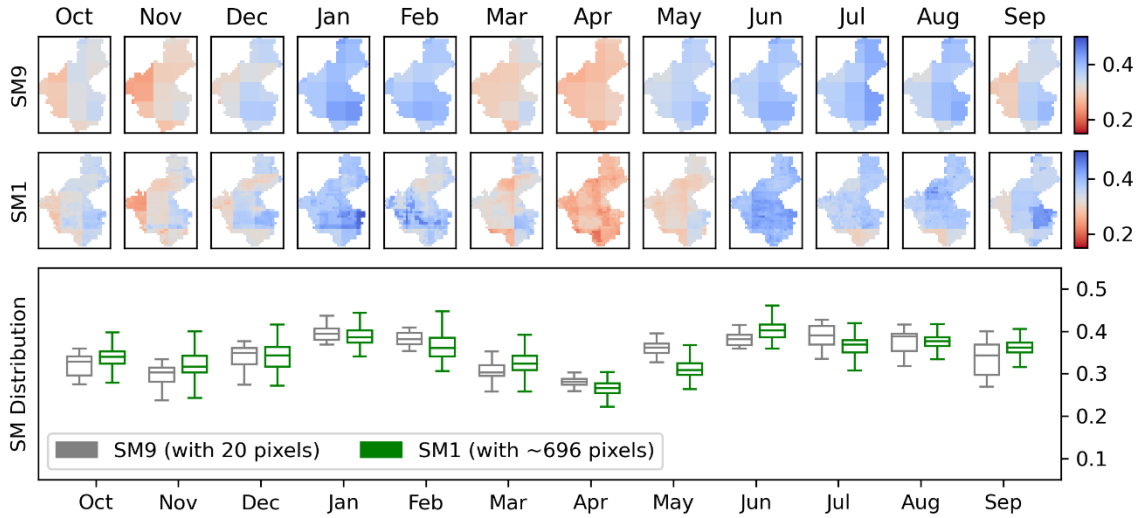

897

898 Figure 6 (top) mapping soil moisture variability at high spatial resolution and (bottom) boxplot of soil moisture distribution for

899 catchment Banyen for the 2015-16 water year.

900

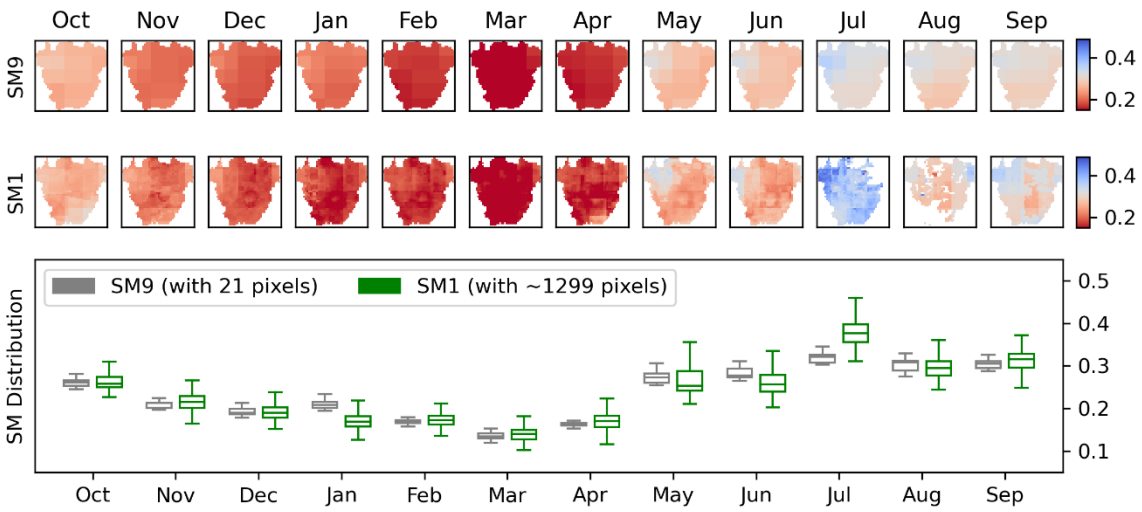

901

902 Figure 7 (top) mapping soil moisture variability at high spatial resolution and (bottom) boxplot of soil moisture distribution for

903 catchment Kh.28A for the 2015-16 water year.

904

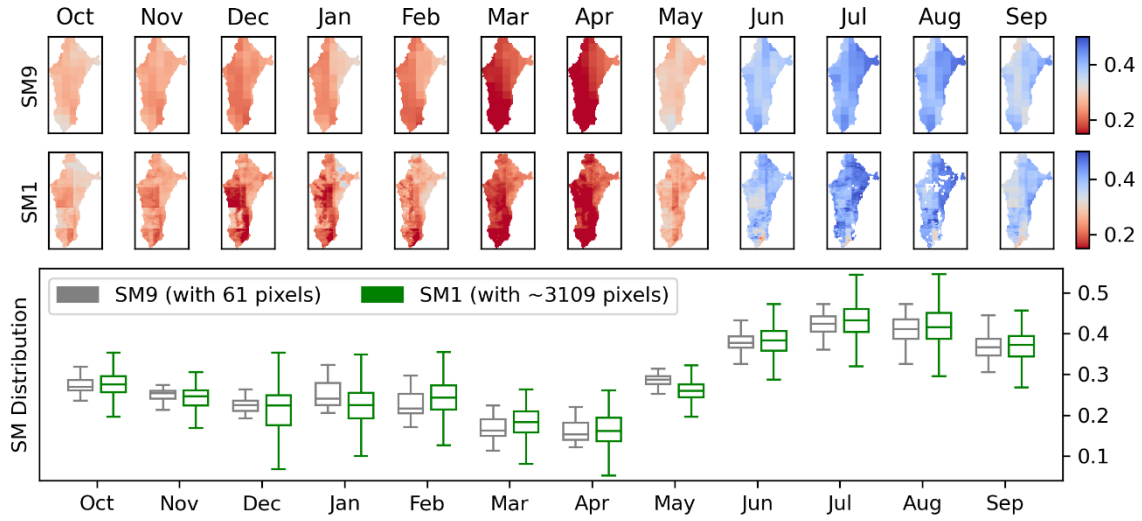

905

906 Figure 8 (top) mapping soil moisture variability at high spatial resolution and (bottom) boxplot of soil moisture distribution for

907 catchment G.8 for the 2015-16 water year.

908

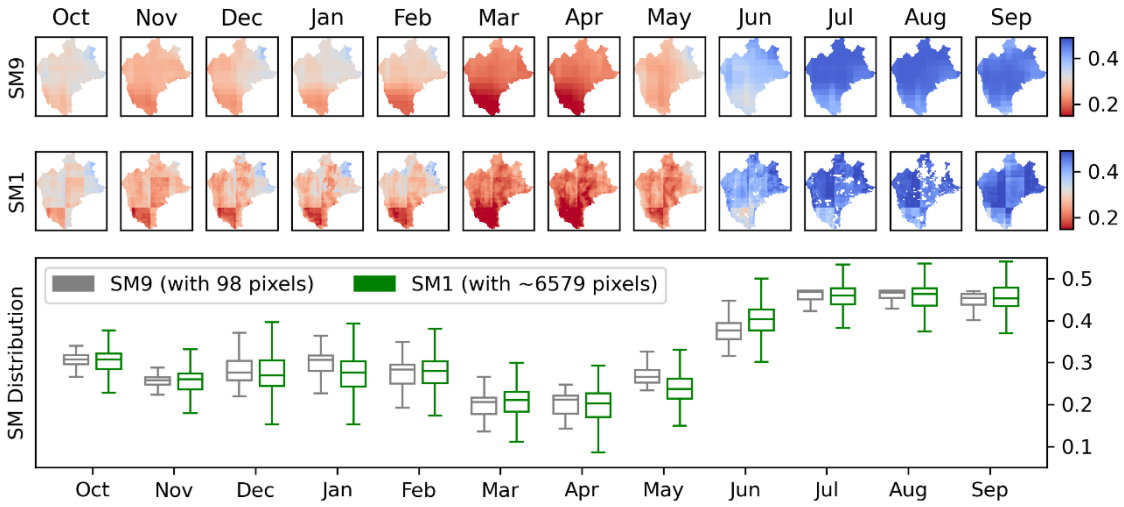

909

910 Figure 9 (top) mapping soil moisture variability at high spatial resolution and (bottom) boxplot of soil moisture distribution for

911 catchment I.14 for the 2015-16 water year.

912

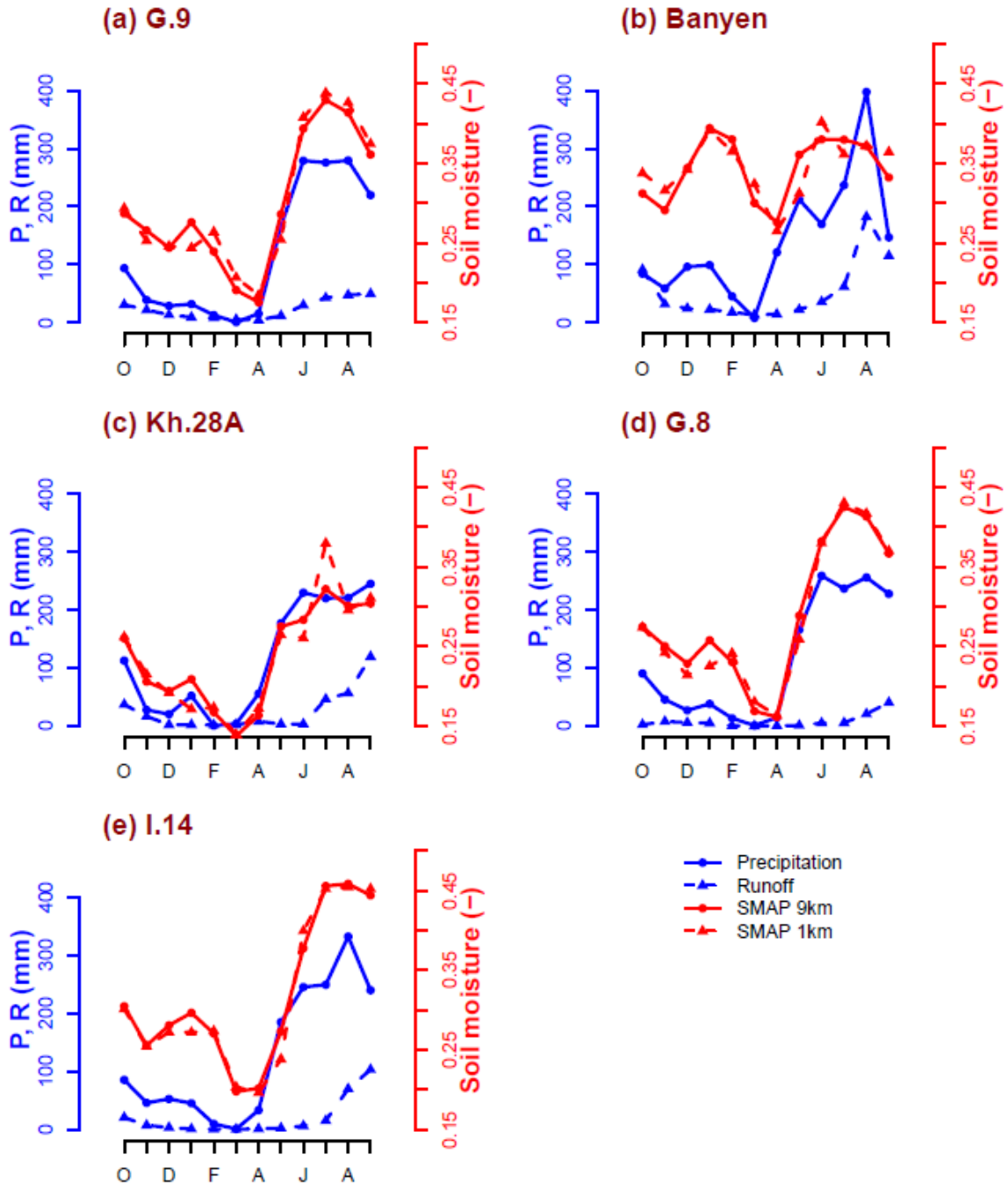

913

914 Figure 10 Variability of precipitation, soil moisture and runoff in (a) G.9, (b) Banyen, (c) Kh.28a, (d) G.8, and (e) I.14 for the 2015-

915 16 water year.

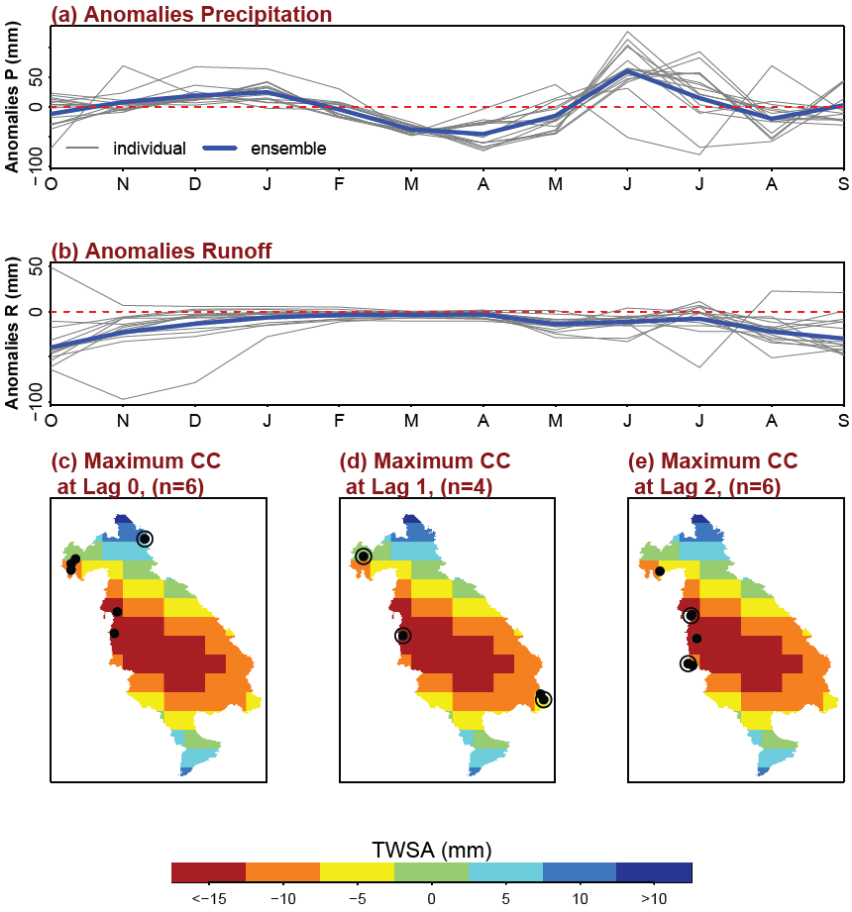

916

917 Figure 11 Comparison of (a) anomalies precipitation, (b) runoff, and (c), (d), (e) relationship between Standardized Streamflow
918 Index (SSI) and Standardized Precipitation Index (SPI). The dash red lines in (a) and (b) represent normal value of the anomalies
919 time series for the 2015-16 water year. The Max CC at lag 0, 1, 2 denote catchments (black dots) having maximum correlation
920 coefficient between SPI and SSI at lag 0, lag1, and lag2 of SPI during 2015-16, respectively. The dots with circles are statistically
921 significant locations at significant level 0.1 for two-sided t-test. The coordinates of catchment locations are taken as the centroids
922 of catchment boundaries. The underlying TWSA maps in (c), (d), (e) are the mean TWSA for the 2015-16 water year extracted
923 from GRACE.

924

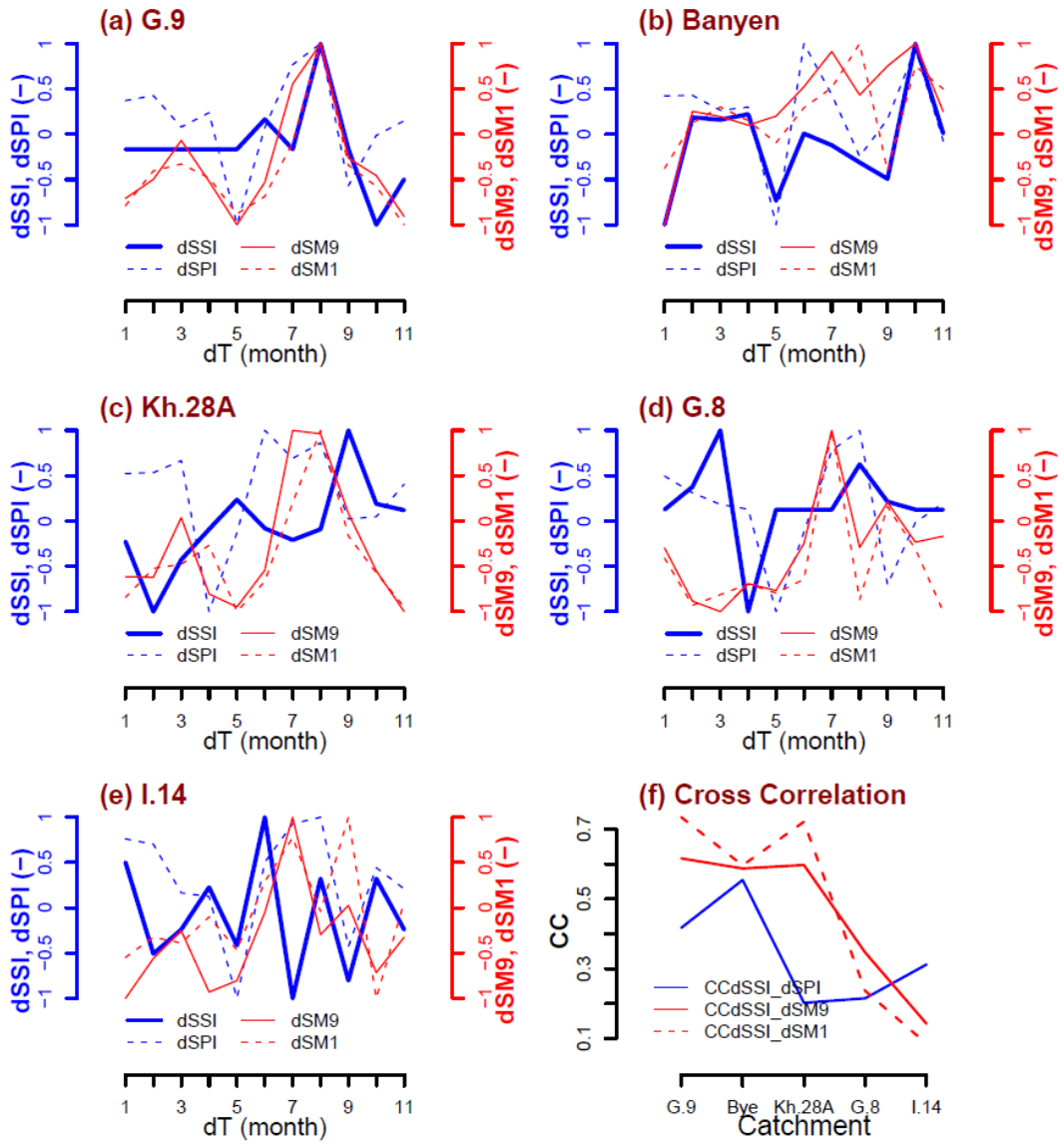

925

926 Figure 12 Monthly changes for the 2015-16 water year in standardized streamflow index (SSI), standardized precipitation index
927 (SPI) and soil moisture for catchment in (a) G.9; (b) Banyen; (c) Kh.28A; (d) G.8, and (e) I.14. The panel (f) presents cross
928 correlation between monthly changes in SPI, SM9, SM1 and monthly changes in SSI for each catchment in (a), (b), (c), (d), and
929 (e).